Andean Geology 46 (3): 445-470. September, 2019
doi: 10.5027/andgeoV46n3-3041

Andean Geology
www.andeangeology.cl

Early Jurassic arc related magmatism associated with porphyry copper mineralization at Zafranal, Southern Peru unraveled by zircon U-Pb ages

***Alan Santos[1, 4], Guo Weimin[2], Fernando Rivera[3], Colombo Tassinari[4], Luis Cerpa[5], Shoji Kojima[1]**

[1] *Universidad Católica del Norte, Av. Angamos 0610, Antofagasta, Chile.*
alanpolo30@gmail.com; skojima@ucn.cl
[2] *Nanjing Center, China Geological Survey, 534 Este Calle Zhongshan, China.*
mwguo@163.com
[3] *Universidad Nacional Mayor de San Marcos, Lima distrito 15081, Perú.*
ing.fernandorivera@hotmail.com
[4] *Instituto de Geociencias de la Universidad de Sao Paulo, Rua do Lago, 526, Sao Paulo Brasil.*
ccgtassi@usp.br
[5] *Instituto Geológico Minero y Metalúrgico, Av. Canadá 1470-San Borja, Lima, Perú.*
lcerpa@ingemmet.gob.pe

** Corresponding author: alanpolo30@gmail.com*

ABSTRACT. Early Jurassic arc-related igneous rocks host porphyry copper prospects and gold-bearing quartz vein deposits in southern Peru. Ten new zircon U-Pb ages for wall rocks of gold-bearing quartz veins, Jurassic rocks and copper-mineralized porphyry bodies in Zafranal porphyry copper, together with published ages for Jurassic rocks, reveal a continuous magmatic evolution of the early Jurassic arc. The Jurassic rocks and gold-bearing quartz vein systems in the western flank of the Western Cordillera are hosted by Paleo- and Meso-proterozoic orthogneisses of the Arequipa Massif (1.75-1.44 Ga) that underwent Grenville-age metamorphism ~1 Ga. The early mafic magmatism is recorded between 199.6-193.2 Ma, and was followed by dominantly felsic magmatism from 184.1-174.9 Ma. Both magmatic events have formed the thinnest intrusive belt (<15 km wide) of the Coastal Batholith in southern Peru. The last magmatic event of the early Jurassic (181.0-174.9 Ma) is represented by several phases of porphyries associated with copper mineralization in the Zafranal porphyry copper deposit. The published ages indicate that the magmatic arc migrated along eastern limit of the Arequipa Massif during Middle Jurassic. In the late Jurassic (~146 Ma) the magmatic locus returned near early Jurassic intrusion. Overall, the plutonic intrusive rocks and porphyry bodies with copper mineralization represent the oldest magmatic events of the Coastal Batholith of Peru formed during the early Jurassic.

Keywords: Coastal Batholith, Zafranal porphyry, Early Jurassic, U-Pb zircon age, SHRIMP.

RESUMEN. Magmatismo relacionado al arco Jurásico temprano asociado con la mineralización pórfido de cobre en Zafranal, Sur de Perú, esclarecido mediante edades U-Pb en circones. Las rocas ígneas relacionadas al arco Jurásico temprano del sur de Perú albergan prospectos de pórfidos cupríferos y depósitos de vetas de cuarzo con contenido de oro. Diez nuevas edades U-Pb en circones de la roca caja de las vetas de cuarzo con oro, rocas jurásicas y stocks porfiríticos con mineralización cuprífera del pórfido de cobre Zafranal, junto con edades publicadas para las rocas jurásicas, revelan una continua evolución magmática del arco Jurásico temprano. Las rocas jurásicas y los sistemas de vetas de cuarzo con contenido de oro en el flanco oeste de la Cordillera Occidental están alojadas en ortogneis del Paleo y Meso-Proterozoico del Macizo de Arequipa (1.75-1.44 Ga) que sufrieron metamorfismo de edad Grenvilliana ~1 Ga. El magmatismo máfico se registra entre 199.6-193.2 Ma, y fue seguido por magmatismo predominantemente félsico desde 184,1-174,9 Ma. Ambos eventos magmáticos han formado el cinturón intrusivo más delgado (<15 km de ancho) del Batolito de la Costa del sur de Perú. El último evento magmático del Jurásico temprano está representado

por varias fases de stocks porfiríticos asociados con la mineralización cuprífera en el pórfido de cobre Zafranal, con emplazamientos durante los 181.0-174.9 Ma. Edades publicadas indican que el arco magmático migró a lo largo del límite este del afloramiento principal del Macizo de Arequipa durante el período Jurásico medio. En el Jurásico tardío (~146 Ma) el foco magmático retornó cerca de las intrusiones del Jurásico temprano. En general, las rocas intrusivas y los stocks porfiríticos asociados con mineralización de cobre representan los eventos magmáticos más antiguos del Batolito de la Costa del Perú que se formaron durante el Jurásico temprano.

Palabras clave: Batolito de la Costa, Pórfido Zafranal, Jurásico temprano, Edades U-Pb en circones, SHRIMP.

1. Introduction

Considerable volumes of magma in the Peruvian convergent margin magmatic-arc, that formed the Coastal Batholith, were generated during a protracted time span (Jenks and Harris, 1953; Cobbing and Pitcher, 1972; Cobbing *et al.*, 1977). Mesozoic plutons were emplaced within metamorphic rocks of Arequipa Massif (Stewart *et al.*, 1974; Cobbing *et al.*, 1977; Casquet *et al.*, 2010). In the Arequipa Segment the emplacement zone (<15 km wide) was controlled by large faults (Caldas, 1993; Demouy *et al.*, 2012). These faults integrated in the Cincha-Lluta fault system, are thought to have generated crustal weakness zones that allowed repetitive injections of magma (Caldas, 1993) and associated copper-gold mineralization (Carlotto *et al.*, 2009a). The mineralization includes gold-bearing quartz veins and porphyry type deposits, and thus a significant number of porphyry copper and associated Mesozoic magmatic-hydrothermal deposits prospects have been identified (Fig. 1). The porphyry copper prospects show a marked tendency to occur in typically orogen-parallel linear belts (Sillitoe and Perelló, 2005) or within magmatic arc (Seedorff *et al.*, 2005). Each belt corresponds to a magmatic arc of broadly similar overall dimensions (Sillitoe, 2010); furthermore, each metallogenic belt migrates systematically farther east, related to the magmatic arc (Sillitoe, 2003). Determining the temporal and spatial evolution of the magmatic arcs of Coastal Batholith (Arequipa Segment; Cobbing *et al.*, 1977), in southern Peru will contribute to our understanding of metallogenic epoch, as a first order approach for exploration targets. According to the geochronological data the Coastal Batholith was considered to have been emplaced in late Cretaceous (Cobbing and Pitcher, 1972; Stewart *et al.*, 1974; Cobbing *et al.*, 1977; Weibel *et al.*, 1978; Cordani *et al.*, 1985; Beckinsale *et al.*, 1985; Mukasa, 1986; Caldas, 1993; Schildgen *et al.*, 2009; Carlotto *et al.*, 2009a), but afterwards divided into two groups one early Jurassic and other Upper Cretaceous (Demouy *et al.*, 2012; Boeckhout, 2012). However, the emplacement of the first magmatic suites of the Coastal Batholith, occur during the early Jurassic and is located from Arequipa to Chuquibamba (Fig. 1). Early Jurassic rocks are registered in southern Arequipa by Mukasa (1986), who considered that the extent of this arc remains unsolved. Thus, more recent studies (Demouy *et al.*, 2012; Boeckhout, 2012) have focused on the Jurassic arc extent close to Arequipa. Therefore, this study aims to determine the early Jurassic arc extent to the northwest of Arequipa and crystallization age of porphyry bodies related to copper mineralization in Zafranal porphyry copper deposit by means of zircon U-Pb ages with sensitive high-resolution ion microprobe (SHRIMP) and laser ablation inductively-coupled plasma spectrometry (LA-ICP-MS) determinations. Furthermore, this paper describes the regional geological setting of Jurassic intrusive rocks (Coastal Batholith-Arequipa Segment), with particular emphasis on the porphyritic bodies that host the copper mineralization in Zafranal, based on more than four years of fieldwork by the authors during a study of the Coastal Batholith program that included 1:25,000-scale regional mapping.

2. Tectonomagmatic setting

The early Jurassic intrusive rocks of southern Peru extends for ~130 km between latitudes 15°48' and 16°36' S and contains copper and gold-bearing mineral deposits, such as porphyry copper and gold-bearing quartz veins (Fig. 1). The oldest rocks within the study area are assigned to the metamorphic Arequipa Massif (Cobbing and Pitcher, 1972) of Proterozoic age (Cobbing *et al.*, 1977; Dalmayrac *et al.*, 1977; Shackleton *et al.*, 1979). This massif represents the site of a complex history of sedimentation, magmatism and metamorphism in the Paleoproterozoic, and development of a sedimentary basin in the Mesoproterozoic (Casquet *et al.*, 2010). The Arequipa Massif was accreted to the western margin

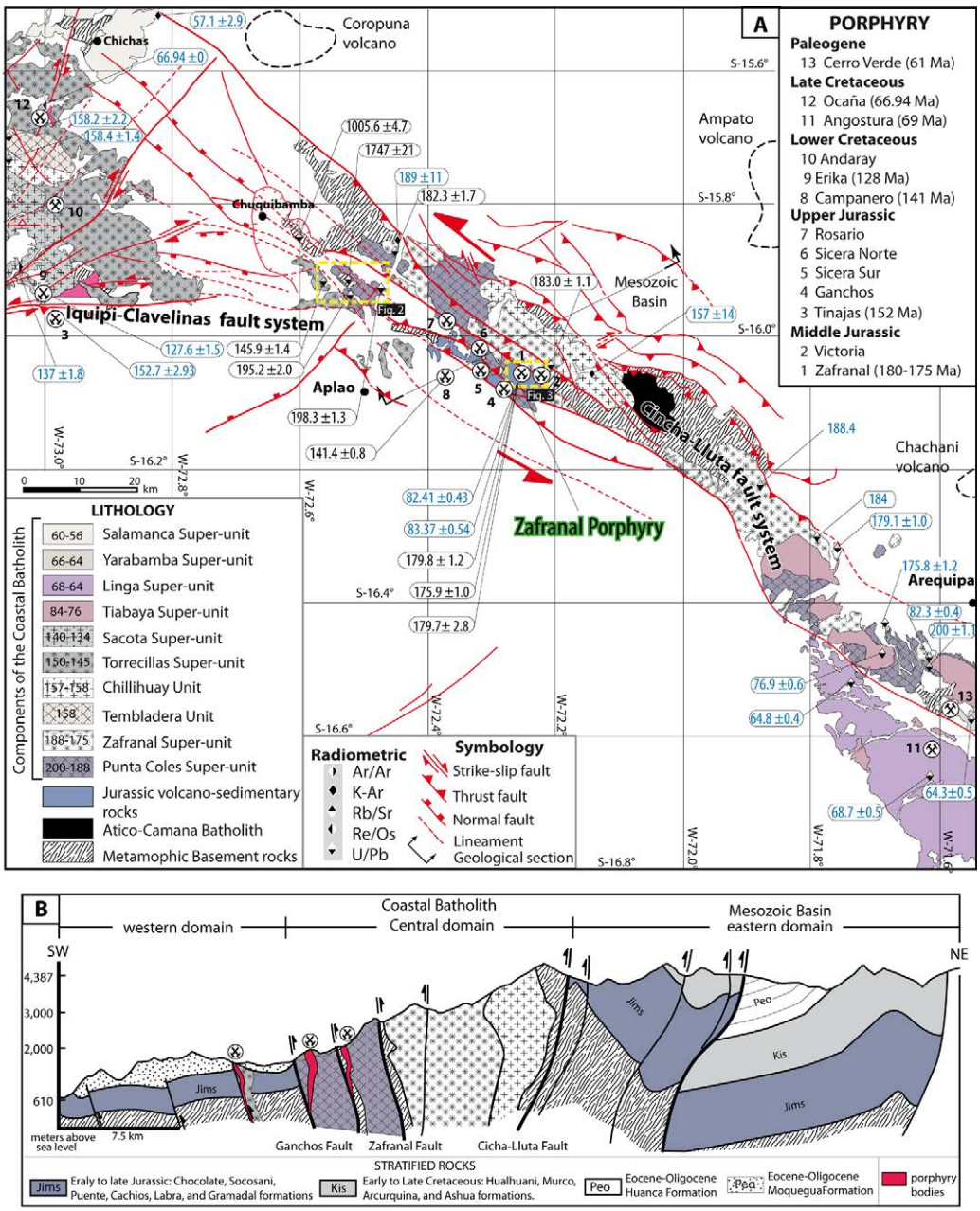

FIG. 1. **A.** Regional geologic map of the northern sector of the Arequipa Segment with the location of the main porphyry copper deposit (modified from Santos *et al*., 2016). The age data of blue letters are compiled from Stewart *et al*. (1974); Cordani *et al*. (1985); JICA (1986); Mukasa (1986); Demouy *et al.* (2012); Rivera (2012a); Huaman *et al.* (2014); Santos *et al*. (2016), and those of black letters are obtained in this work. **B.** Geological section. The location is in map.

of Gondwana, in the late Proterozoic related to the Sunsas orogeny (Wasteneys *et al.*, 1995; Loewy *et al.*, 2004; Chew *et al.*, 2007; Ramos, 2008). Following, terrane accretion, between 850 to 650 Ma the Andean margin of Peru was quiescent (James, 1971; Chew *et al.*, 2008; Acosta and Sempere, 2017). During in the Early Paleozoic (Ordovician and Silurian-Devonian) it was affected by extensive

tectonic events and development of coast-parallel magmatic arcs (Shackleton *et al.*, 1979; Mukasa and Henry, 1990; Bahlburg *et al.*, 2006; Reitsma, 2012). Subsequently, Permian-Triassic rifting along the western margin of Gondwana marks the beginning of the Andean orogenesis (Davidson and Mpodozis 1991; Benavides, 1999).

Since *ca.* Mid-Mesozoic (200-90 Ma), the Andean evolution seems to be more directly controlled by plate convergence (Coira *et al.*, 1982; Thorpe, 1984; Allmendinger *et al.*, 1997; Ramos and Aleman, 2000). It was dominated by periods of intracontinental rifting (Petford and Atherton, 2003) and formation of a well-defined intra-arc and back-arc basins (Coira *et al.*, 1982; Atherton *et al.*, 1983; Davidson and Mpodozis, 1991). Mesozoic intra-arc and back-arc rifts were filled vertically up through axial faults by magmas derived from the upper mantle or lower crust (Couch *et al.*, 1981; Atherton *et al.*, 1983, 1985), as well as sedimentary detritus derived from the rift margins, volcanic edifices (Benavides, 1956) and locally interbedded calcareous sedimentary rocks (Benavides, 1962). Marine sedimentation continue more or less uninterruptedly from the Jurassic into the early Cretaceous (Benavides, 1956). The rifting along the western margin of Peru were controlled by regional-scale axial fault systems, which correspond to the NW-striking Cincha-Lluta Fault System (CLFS) (Carlotto *et al.*, 2009a; Simmons *et al.*, 2013), which was active during batholith construction (Demouy *et al.*, 2012). This fault system is equivalent to the Icapuquio Fault System (IFS) farther south in Peru (Wilson and García, 1962; Vargas, 1970; Vicente *et al.*, 1979; Jacay *et al.*, 2002), which controls the spatial distribution of most of the porphyry Cu-Mo deposits, including the Zafranal porphyry district (Fig. 1). Furthermore, Zafranal porphyry copper is located very close to the intersection with the Iquipi-Clavelinas Fault System (ICFS) of EW orientation.

The late Cretaceous-Paleocene (90-52 Ma), Peruvian continental margin was dominated by compressional tectonics (Isacks, 1988, and references therein; Camus, 2003). This marks the beginning of crustal thickening (Vicente, 1989; Jaillard, 1992; Carlotto *et al.*, 2009b), produced by structural shortening of the crust and uplift due to thermal thinning of the lithosphere by delamination (James, 1971; Isacks, 1988; Sobolev and Babeyko, 2005; Oncken *et al.*, 2006; Wipf, 2006). The old fault systems (CLFS and IFS) changed from normal to reverse thrust regime, and as a result the magmatic arc installed within the Arequipa Massif begins to uplift and separates the Arequipa Basin from the ocean (Carlotto *et al.*, 2009a), starting the accumulation of the entirely subaerial volcanic rocks linked to Toquepala Group (Clark *et al.*, 1990a). Plutonic bodies of the Yarabamba Super-unit (Coastal Batholith) intruded the Toquepala Group (Stewart *et al.*, 1974; Mukasa, 1986; Beckinsale *et al.*, 1985; Boily *et al.*, 1989; Clark *et al.*, 1990a; Martínez and Cervantes, 2003), and obscured much of the earlier rift sequence and late Cretaceous fold-and-thrust belt. Porphyry copper deposits are associated with Paleocene and Early Eocene granite and granodiorite porphyry stocks (Simmons *et al.*, 2013).

Eocene-Oligocene (52-30 Ma), the tectono-magmatic events were controlled by the evolution of a flat-slab subduction regime (Sandeman *et al.*, 1995; Noury *et al.*, 2017), which caused a farther northeast migration of the locus of magmatism (Andahuaylas-Yauri Batholith; Sandeman *et al.*, 1995; Perelló *et al.*, 2003). Furthermore, uplift in the Precordillera, the Arequipa Massif is overturned and thrusted over the Mesozoic rocks (Vicente, 1989; Caldas, 1993), followed by erosion-degradation of the older magmatic arc and Jurassic basin allowed the development of the syn-orogenic Querque foreland and Moquegua forearc basins (Vicente, 1989; Jaillard, 1992; Carlotto *et al.*, 2009b).

Early Miocene (24-17 Ma), extensive explosive volcanism of the Huaylillas Formation mantled the degradational Altos de Camilaca surface recorded in the Moquegua Formation (Tosdal *et al.*, 1981, 1984; Quang *et al.*, 2003, 2005). A late Miocene to Holocene, phase of Andean uplift (Isack, 1988; Roperch *et al.*, 2006), was accompanied by widespread ignimbrite eruptions of the Chuntacala Formation (14-8 Ma), and andesitic volcanism of the Pliocene-Holocene Barroso Group (<5 Ma) and exhumation of the giant porphyry copper deposits (Tosdal *et al.*, 1981, 1984; Clark *et al.*, 1990b; Quang *et al.*, 2005), based on the size classification proposed by Clark (1993).

2.1. Tectonics and stratigraphy

Arequipa Segment of the Coastal Batholith comprises three main tectonic domains bounded by high-angle NW-striking faults (Fig. 1). The eastern domain, east of the Cincha-Lluta Fault System (CLFS), contains basement blocks, composed of migmatite

and gneiss (Wasteneys *et al*., 1995). These basement blocks, were intruded by diorites, sienogranites-monzogranites of Ordovician age (466.1±2.6 Ma; Santos *et al*., 2016). Both the basement and intrusive rocks are overlain by volcanic breccias and andesitic flows of Chocolate Formation, and limestones of Socosani Formation (Romero and Ticona, 2003). Towards the Mesozoic Basin (Fig. 1B), the sedimentary outcrops are approximately >5 km thick (Romero and Ticona, 2003), divided into Chocolate, Socosani, Puente, Cachios, Labra, Gramadal, Hualhuani, Murco, Arcurquina, and Ashua Formations, which are strongly deformed showing sub-isoclinal folds, vertical and overturned strata. These strata are unconformably overlain by >2 km-thick of conglomerates, sandstones, and some volcanic breccias of the Huanca Formation (Querque Basin). The main Cincha-Lluta fault is characterized by high-angle NE-emergent, NW-striking, reverse fault and with a sinistral component.

The central domain (Fig. 1B), is located farther west of the Western Cordillera, and here, the basement rocks (Arequipa Massif) are intruded by plutonic complexes of the Coastal Batholith. These rocks together have an elongate geometry with orientation N145°, parallel to the main faults and orogen of NW-orientation. Furthermore, in areas where intrusive rocks were cut by sinistral faults, many mylonites and shear zones occur in some place. There are roof pendants of basement rocks (*e.g.,* Cerro Gandolfo; Fig. 2), as well as volcano-sedimentary sequences of the Chocolate Formation (*e.g.,* Zafranal porphyry). Plutonic rocks, ranging in composition from diorites and granites through quartz diorites to tonalites-granodiorites, were emplaced throughout the Arequipa Massif of relatively variable large to short pulses, each estimated to last roughly 4 to 12 Ma (Pitcher, 1985; Santos *et al.*, 2016).

In the western domain, the Mesozoic rocks are covered by sedimentary rocks of the Moquegua Formation (Fig. 1B). This unit comprises mainly conglomerates, sandstones, siltstones with evaporite intercalations and tuffs with ages K-Ar of 25.3 to 22.8 Ma (Tosdal *et al.*, 1981; Quang, 2005). A number of high-angle reverse faults of the Western Andean Escarpment cut both Mesozoic sedimentary bedrock and lower Moquegua red beds. Near the town of Aplao, a reverse fault dipping approximately 70° NE places Chocolate Formation over lower Moquegua, but deformation decreases up section, with upper Moquegua group strata deformed into a monocline and erosionally stripped (Schildgen *et al.*, 2009). In the early Miocene (23-17 Ma), ignimbrite flows of the Huaylillas Formation were deposited on the surface of erosion of the Moquegua Formation (Tosdal *et al.*, 1981; Quang *et al.*, 2005).

3. Regional geology of ore deposits

The studied area is a thin strip (<15 km wide) of rocks belonging to the Coastal Batholith. This area contains gold-bearing quartz veins hosted in metamorphic and volcano-sedimentary rocks, and porphyry copper deposits (Fig. 1).

3.1. Intrusion-related gold-bearing quartz vein systems

Vein-type deposits are by far the most abundant and common mineralization style in the Coastal Cordillera (Sillitoe, 2003). The Rinconada de Chapi and Copacabana mining districts are located in the Quebrada Ongoro, 18 km southeast of the town of Chuquibamba (Figs. 1A and 2), and include gold-bearing quartz vein mineralization (*e.g.,* Palpa-Ocoña, southern Peru; Sillitoe and Thompson, 1998). These quartz veins occur as NW-SE strycking swarms and with NEE-SWW orientations related to the main fault systems (CLFS and ICFS). In Copacabana, the gold-bearing quartz veins have the orthogneiss of the Arequipa Massif as wall rocks. These orthogneiss show a granoblastic texture, whit quartz, K-feldspar and plagioclase with biotite in thin bands and lenticular structures. The mineralization occurs as tabular quartz veins (dips >60°S), with a marked structural control in a N70°E trend. The major veins are 0.3 to 0.5 m thick. They consist mainly of quartz containing pyrite, chalcopyrite and native gold, and as supergene mineral contain hematite, goethite and copper-oxides (mainly chrysocolla). The higher grades range from 10 to 12 g/t Au. Hydrothermal alteration of the host rocks is common in many areas around the quartz veins, and consists of kaolinization and subordinate chloritization. At Rinconada de Chapi the veins are hosted in a volcano-sedimentary sequence and dikes complex intensely deformed, as indicated by vertical and overturned strata, anastomosing and thrust-bounded tectonic lenses of the Chocolate Formation. The ore deposits occur as steep-dipping tabular quartz veins (dips >80°N), with marked structural control and discontinuous longitudinal development in a NW-SE

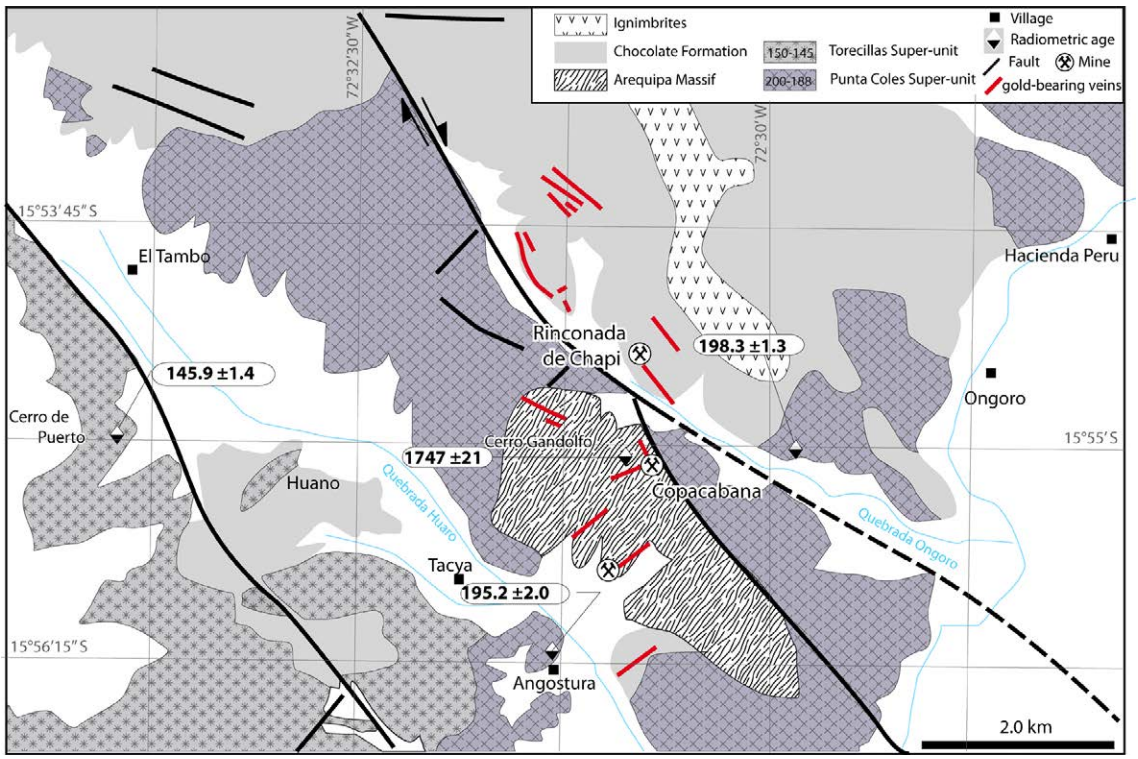

FIG. 2. Arequipa Massif and Chocolate Formation rocks-hosted gold-bearing quartz veins and controlling faults in the Quebrada Ongoro (Modified from INGEMMET, 2001). Radiometric age obtained in this work. Map location is in figure 1.

direction (N140°) reaching 1 km along strike. The major quartz veins are <0.8 m thick. They consist mainly of quartz, pyrite, chalcopyrite and native gold, and as secondary mineral contains calcite, hematite, chrysocolla and malachite. The higher grades range from 10 to 15 g/t Au. Also there are some thin veins (<10 cm), with quartz and galena.

Rocks of the Arequipa Massif and Chocolate Formation were intruded by diorites to quartz diorite of the Punta Coles Super-unit, cropping out largely in the Quebrada Ongoro, but also to the northeast part of gold-bearing quartz vein district. Based on the fact that the diorite-quartz diorite intrusive truncates the gold-bearing quartz veins hosted in rocks of the Arequipa Massif, it is inferred that the formation of these mineral deposits occurred before the emplacement of the dioritic-quartz dioritic intrusive (Cerro Gandolfo, Fig. 2). The bulk of the Punta Coles super-unit is made up of light- to medium-dark gray to greenish, hypidiomorphic granular diorite in the central part (following IUGS classification, Streckeisen, 1973), towards the boundaries increases the quartz content and reduces its grain size (Quebrada Ongoro). In general, these rocks are composed of a dominance of plagioclase over chloritized amphibole and traces of biotite. Minor quartz and sericitized K-feldspar occur interstitially in the equigranular phase.

3.2. Zafranal porphyry copper

The Zafranal porphyry copper deposit is located approximately 90 km northwest of the city of Arequipa in southern Peru, it was first described by Tejada (2010). Measured and indicated resources amount >472.1 Mt, 0.36% Cu and @ 0.08 g/t Au (Fernandez-Baca, 2011). The Zafranal local geology was described by geologists of AQM Peru S.A.C. (De Ruijter *et al.*, 2013) and summarized by Rivera *et al.* (2010), Rivera (2012a, b). Metamorphic rocks of the Arequipa Massif are the oldest rocks at Zafranal, cropping out largely along the shear zone of the NW-striking Zafranal reverse fault. The next younger units are volcano-sedimentary sequences of the Chocolate Formation comprised of sandstone and

siltstones, which in turn are overlain by tuffs, breccias and andesitic lava flows (Rivera *et al.*, 2010; Fig. 3), which are present as roof pendants in igneous intrusions. Several roof pendants and large blocks of volcano-sedimentary sequences are present in the pre-mineralization diorites-granodiorites, which form the northern margin of the Zafranal porphyry. Alteration and mineralization at Zafranal is centered on porphyritic dykes and stock complexes, ranging in composition from diorite to quartz diorite, which show potassic alteration dominated by biotite (Tejada, 2010). The older porphyry suite (Zafranal diorite) host copper mineralization, displaying intense sericitic alteration overprinted on potassic alteration (Rivera *et al.*, 2010), including typical A-type chalcopyrite-pyrite and B-type chalcopyrite-molybdenite quartz veinlets, and D-type quartz-pyrite-chalcopyrite veinlets with sericitic halos (cf. Gustafson and Hunt, 1975). An outer propylitic halo with epidote-chlorite, approximately 400 m wide, is present to the north (Rivera, 2012a). A $^{40}Ar/^{39}Ar$ plateau age of 82.41±0.43 Ma was obtained for hydrothermal biotite of the Zafranal diorite (Rivera, 2012a), located close to the east of the Zafranal porphyry system (Fig. 3). A microdiorite porphyry cut the Zafranal diorite, and is characterized by a much weaker potassic alteration towards depth, sparse A-, and B-type veinlets, containing 0.35-0.40 percent Cu in the hypogene mineralization (Rivera *et al.*, 2010). A $^{40}Ar/^{39}Ar$ plateau ages of 83.370±0.54 and 81.16±0.43 Ma were obtained for hydrothermal biotites (Rivera, 2012a), in a microdiorite located in the central part of the Zafranal porphyry system (Fig. 3). Post-mineral intrusions diorite and diorite-monzodiorite dykes, displaying only weakly propylitic alteration with pyrite and chalcopyrite dissemination (Rivera, 2012a). However, U-Pb data presented herein demonstrates that the porphyries are temporally related to an early Jurassic magmatism.

Hydrothermal alteration and mineralization. Zafranal porphyry partly conform to the classic Lowell and Guilbert (1970) hydrothermal alteration zonation model, in which a potassic altered core grade laterally to an annular sericitic zone surrounded by a fringe of propylitic alteration (Rivera *et al.*, 2010). The potassic alteration is defined by the presence of hydrothermal biotite, quartz and K-feldspar together with anhydrite, chalcopyrite±pyrite, and molybdenite, which make up the hypogene mineralization (Rivera, 2012a). Hornblende and magmatic biotite in the igneous rocks are almost totally replaced by fine-grained, brown biotite, and plagioclase is partially replaced by K-feldspar. The sericitic alteration clearly overprinted and destroys the earlier formed potassic assemblage and comprises quartz, sericite, and pyrite.

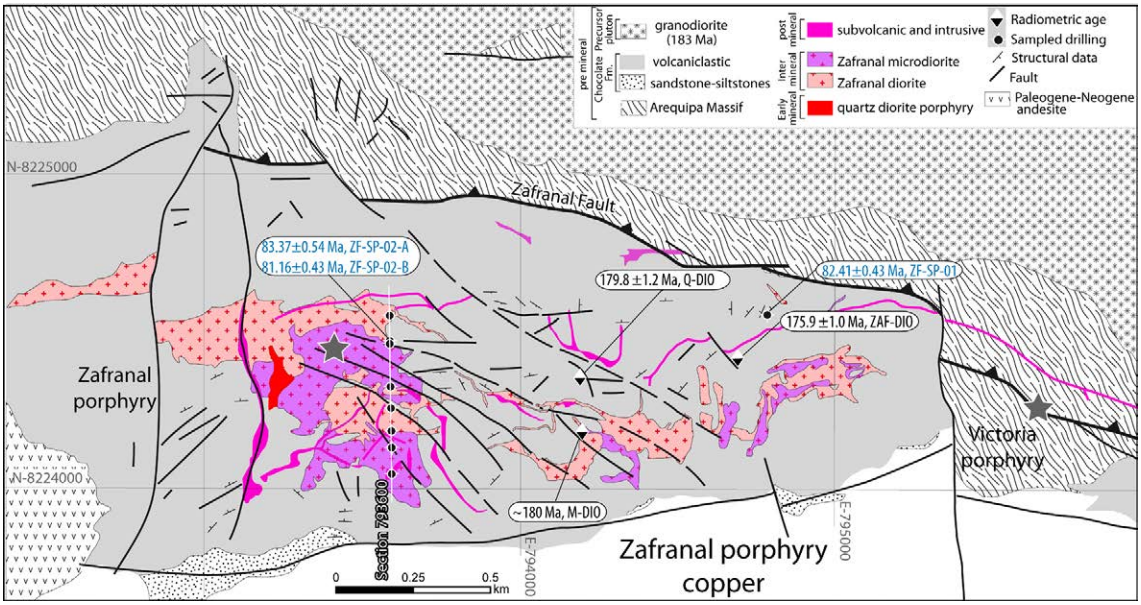

FIG. 3. Geologic map of Zafranal porphyry copper (De Ruijter *et al*., 2013). The age data in blue letters are compiled from Rivera (2012a) and those in black letters are obtained in this work. Map location is in figure 1.

Chalcopyrite is partially replaced by supergene chalcocite and covelite (Tejada, 2010). Intermediate argillic alteration is characterized by the presence of illite, chlorite and sericite together with kaolinite and smectite. Locally, internal parts of the southern limit of the deposit contain quartz, alunite, kaolinite and illite, minerals denoting the existence of advanced argillic alteration.

Supergene alteration and mineralization. The upper oxidized zone averages ~60 m thick, which is located within the leached capping (30-200 m thick), associated with the zone of sericitic alteration (Rivera *et al.*, 2010). In the oxidized zone, chrysocolla, malachite, chalcanthite and neotocite are the ore minerals. The supergene enriched blanket average ~75 m thick, but locally attains a maximum of 150 m (Rivera *et al.*, 2010), where the chalcocite and covellite occur as replacement coating on chalcopyrite, and minor pyrite grains. This supergene profile contains copper grades from 0.8 to 1% (Tejada, 2010).

3.3. Late intrusions

At Cerro de Puerto (Huano village, Fig. 2), a NW elongated pluton composed of hypidiomorphic, granular, amphibole-rich tonalite (Torrecillas Super-unit, Fig. 1), extends from Chuquibamba up to northern Aplao. This pluton is cropping out close to Campanero porphyry copper prospect. The Campanero porphyry prospect (Rivera *et al.*, 2008) is located approximately 14 km west of the Zafranal porphyry (Fig. 1).

Quartzite and siltstone of the Labra Formation are the oldest rocks at Campanero prospect, cropping out largely in the Rio Majes, but also in the central part of the prospect. Pre-mineralization granodiorite-tonalite are widely distributed to the northwest of the prospect. Copper mineralization is spatially and temporally related to a hornblende-rich quartz diorite with porphyritic texture. It presents high content of plagioclase, biotitized amphibole, and quartz. In general, the outcrops present strong sericitic alteration with hematite dissemination in matrix and veinlets. A $^{40}Ar/^{39}Ar$ plateau age of 141.4±0.8 Ma was obtained in hydrothermal biotite (Rivera, written communication, 2016).

4. Sampling at Zafranal Porphyry copper deposit

Sampling was conducted mainly in two transects (Fig. 1) and 10 representative samples of metamorphic and plutonic rocks as well as intrusives associated with porphyry copper mineralization in Zafranal deposit were selected for the U-Pb dating. Sample locations are shown in figure 1. Coordinates, unit, description, abbreviated mineralogy and the analytical work carried out on each sample are presented in table 1. Unit designations is following the nomenclature proposal of Cobbing *et al.* (1977) and Santos *et al.* (2016) (see Fig. 1).

5. Analytical method

New U-Pb ages were obtained using a sensitive high-resolution ion microprobe (SHRIMP) at the Institute of Geosciences of the University of Sao Paulo-Brazil and laser ablation inductively coupled plasma spectrometry (LA-ICP-MS) at the Laboratory of China University of Geosciences (Wuhan).

Zircons grains were separated by standard procedures; including crushing, Wilfley table and a magnetic separation (Frantz), and gravimetric separation by dense liquids to obtain a zircon concentrate. Finally zircon grains were hand-picked under a binocular microscope. A representative set of zircons grains (including the different morphologies of each zircon population) were arranged in rows in a mounting tablet, and fixed with epoxy resin and were polished to standardize the external surfaces. Cathode-luminescence (CL) SEM images, were used to decipher the internal structures of the sectioned grains and to target specific areas within the zircons. The U-Pb isotope analysis were made, using a sensitive high-resolution ion microprobe (SHRIMP) in the same technique described by Sato *et al.* (2014) and laser ablation inductively coupled plasma spectrometry (LA-ICP-MS), the analytical method is reported in Liu (2011). Concordia ages and diagrams were generated using the Isoplot/Ex V.2.49 software package by Ludwig (2001). U-Pb data obtained are in Appendix (Table A1-A2) and results are described below as shown in figures 4-7.

6. Zircon SHRIMP and LA_ICP-MS samples and results

6.1 Wall rock and gold-bearing quartz vein mineralization

Wall rock. A granoblastic orthogneiss (sample 76, table 1) at Copacabana, taken from the wall rock of the quartz veins. The zircons from this sample

TABLE 1. SHORT DESCRIPTION OF ROCKS SELECTED FOR U-Pb ZIRCON DATING.

Sample	Coordinates		Unit	General location	Rock type*	Abbreviated mineralogy**	Analytical work
76	72°31'15.89'' S	15°54''54.19'' W	AM	Cerro Gandolfo	otrhogeneiss	Kfs, Qtz, Pl, Bt-Spn, Zrn-Ser, Ep, Chl, Qtz	L
77	72°36'31.05'' S	15°51'07.91'' W	AM	Cerro Francisco	otrhogeneiss	Otz, Kfs, Bt, Am, Pl-Grt, Ap, Zrn-Qtz, Chl, Ep	L
75	72°29'23.40'' S	15°55'19.97'' W	PC	Cerro Ongoro	quartz diorite	Pl, Qtz-Am, Spn, Bt-Ep,Chl, Ser	L
82	72°31'17.46'' S	15°56'11.80'' W	PC	Village Angostura	diorite	Pl, Am-Bt, Qtz, Spn, Fsp-Chl, Ser, Ep	L
89	72°27'09.88'' S	15°52'07.40'' W	Zaf	Village Andamayo	tonalite	Pl, Qtz, Bt, Kfs-Am, Zrn-Chl-Ep	L
95A	72°12'16.81'' S	16°02'22.59'' W	Zaf	Victoria prospect	granodiorite	Pl, Qtz, Kfs, Bt-Am, Zrn, Fsp-Chl-Ep	L
Q-DIO	72°15'09.66'' S	16°02'46.58'' W	-	[a]Zafranal porphyry	quarzt diorite	Pl, Kfs, Qtz-Am, Bt, Zrn, Ap-Ser, Chl, Qtz II, Spn, Ep	S
ZAF-DIO	72°14'53.55'' S	16°02'44.32''W	-	[b]Zafranal porphyry	quarzt monzodiorite	Pl, Qtz, Kfs-Ap, Zrn, Fsp, Am, Bt-Chl, Ser, Qtz II, Spn, Ep, Bt II	S
M-DIO	72°15'09.69'' S	16°02'52.92'' W	-	[c]Zafranal porphyry	microdiorite	Fsp, Qz-Am-Chl-Ser-Bt II	S
86	72°33'50.51'' S	15°54'57.77'' W	Tor	Cerro Puerto	tonalite	Pl, Am, Qtz-Kfs, Spn, Bt-Ser, Ep, Chl	L

Analytical work : **L** = U-Pb LA-ICP-MS; S = U-Pb SHRIMP.

Unit : **AM** = Arequipa Massif; **PC** = Punta Coles Super-unit; **Zaf** = Zafranal Super-unit; **Tor** = Torconta Super-unit, according to Cobbing *et al.* (1977) and Santos *et al.* (2016).

General location : samples from drill hole **a** = ZFDDH10-024, depth 230 m; **b** = ZFDDH10-125, depth 600 m; **c** = ZFDDH11-166, depth 650 m.

* : Following IUGS classification, Streckeisen (1973).

** : Mineral abbreviations according to Siivola and Schmid (2007) and Kretz (1983).

are equant elongate, to sub-round in shape and less than 200 µm length. The CL images show large relict cores sub-round in shape, in some cases present igneous zoning, surrounded by mantles of variable thickness with homogeneous zoning rims, discordant to the earlier oscillatory zoning (Fig. 4A). Twenty spots were analyzed on 20 zircon grains, included cores and rims. Six of eleven cores plot near concordia and yield a mean U-Pb age of 1747±21 Ma (MSWD=6.8), which is interpreted as the crystallization age of the igneous protolith. The very high Th/U values of cores (1.69-1.05), typical of igneous zircons (Hoskin and Schaltegger, 2003), reinforce this interpretation. The remaining nine zircons were analyzed in the rims yielded U-Pb ages between 1594-1076 Ma, the rims are high-U (mostly over 311-1240 ppm) and with low Th/U ratios (mostly <0.9) indicative of an igneous origin with partially recrystallized rims. This decrease correlates with a decrease in the $^{207}Pb/^{206}Pb$ age of the zircon (Hoskin and Schaltegger, 2003).

The other sample of granoblastic orthogneiss (sample 77, table 1) from approximately 2 km southeast of the Chuquibamba (Fig. 1); The zircons from this sample are sub-round in shape and less than 170 µm length. The CL images reveal small few relict cores, some cores preserve igneous zoning, and other cores show low-luminescence, in both cases the cores are girded by areas broad and homogeneous (Fig. 4B). Twenty spots were analyzed on 20 zircon

grains. Three cores yielded U-Pb ages between 1444-1383 Ma, containing zircon Th/U ratios from <0.7. The rims yielded U-Pb ages 1236-827 Ma, if the more imprecise rims analyses are excluded, the rest plot yielded a zircon U-Pb age of 1005.6±4.7 Ma (MSWD=5.5), containing low Th/U ratios from 0.80 to 0.23. This calculated age probably corresponds to a Grenvillian metamorphism age that started at *ca.* 1 Ga (Casquet *et al.*, 2010), whereas the igneous protolith have crystallized in the Mesoproterozoic (1444 Ma).

Post-mineral rocks in gold-bearing quartz vein mineralization area. An equigranular quartz diorite (sample 75, table 1) from approximately 2.5 km southeast of the main quartz veins (Quebrada Ongoro, Fig. 2). Separated zircons are mostly 150 μm in length, equant to slightly elongated, and sub-round in form. CL images display an oscillatory zoning (Fig. 4C), yielded a zircon U-Pb age of 198.3±1.3 Ma based on fourteen of twenty zircon crystals, with Th/U from 1.4 to 3. Six crystals excluded from the age calculation; one zircon is very old, the textural features and isotopic measurements indicate this crystal is an inherited xenocryst dated at 1583±47 Ma, with a zircon Th/U ratio (0.94), probably incorporated from the Arequipa Massif (Fig. 4C). The other sample of diorite (sample 82, table 1) from village of Angostura (Quebrada Tacya, Fig. 1). The zircons from this sample are sub-round to elongated grains (less than 120 μm in length). The CL images show a slight oscillatory zoning towards the edges; many grains generally have clear cores. Based on ten spots of twenty grains analyzed, yielded a zircon U-Pb age of 195.2±2.0 Ma, with zircon Th/U ratios from 1 to 2.1. Ten spots analyses were excluded from the calculated age, as yielded discordant dates (Fig. 4D).

Zircon spot U-Pb analyses from regional equigranular tonalite (sample 89, table 1), collected from village of Andamayo (Río Colca). Eight of twenty analyzed zircons yield an age of 182.3±1.7 Ma (Fig. 4E).

6.2 Zafranal porphyry copper

The denomination of the different magmatic phases (precursor, pre-, inter-, and post-mineralization) were made during the geological mapping and drill-core logging stages, performed by geologists of AQM Peru S.A.C. and summarized by Tejada (2010), Fernandez-Baca (2011), Rivera *et al.* (2008, 2010), Rivera (2012a, b), and De Ruijter *et al.* (2013). This observation has allowed to obtain relative ages, and here were included the approximate duration of different porphyry bodies related to the copper mineralization in Zafranal, determined by using exclusively U-Pb zircon dating.

Precursor pluton. A hypidiomorphic granular granodiorite (95A, Zafranal Super-unit) at the Zafranal porphyry district, taken from approximately 4 km east of the center Zafranal porphyry and 2.5 km northwest of the Santo Domingo mining (gold-bearing quartz veins). In general it consists of slightly NW elongated pluton (Fig. 1), which extends to Cerro Torconta and reach the south of Arequipa. Based on field relations, the granodiorite intruded to gneiss and early diorites. The zircons of granodiorite are elongate (less than 210 μm in length) euhedral in shape. CL images show that most crystals with a prominent oscillatory zoning in the entire zircon population, but some few grains show core and rims with low-luminescence (Fig. 5A). The granodiorite yielded a U-Pb age of 183.0±1.1 Ma (Fig. 5A), based in eleven zircons of twenty points analyzed. Three spot analyses yielded younger dates (178 Ma), presumably due to Pb loss. The all crystal zircons analyzed display high-U (810-1900 ppm) and low Th/U values (0.5-0.8).

Early-mineral rocks. A quartz diorite porphyry (Q-DIO) at the Zafranal porphyry, taken from approximately 0.5 km east of the center of the porphyry copper (Fig. 3) present lower degree of hydrothermal alteration. The zircon crystals from this sample generally are clear and colorless and mostly elongate (less than 400 μm in length) sub-rounded to euhedral in shape, this combination of zircon shape suggests relatively rapid to moderate crystallization with a high-level emplacement. The CL images reveal an ocillatory zoning and some irregular zoning, but one zircon xenocrystal has internal structure different from the remaining ninteen zircons. The xenocrystal has homogeneous CL, with outermost invariably being a bright CL rim. Therefore, largely given the common nature of the zircon population. The quartz diorite porphyry, yielded a zircon U-Pb age 179.8±1.2 Ma (Fig. 5B), based on twelve of nineteen. Six zircons are younger due to Pb loss. The xenocrystal indentified in CL is much older, isotopic measurements indicate that it is an inherited xenocrystal dated at 1032±11 Ma, with low-U (350 ppm) a low-Th/U ratio (0.51), similar in age to those of the Arequipa Massif (Fig. 5B).

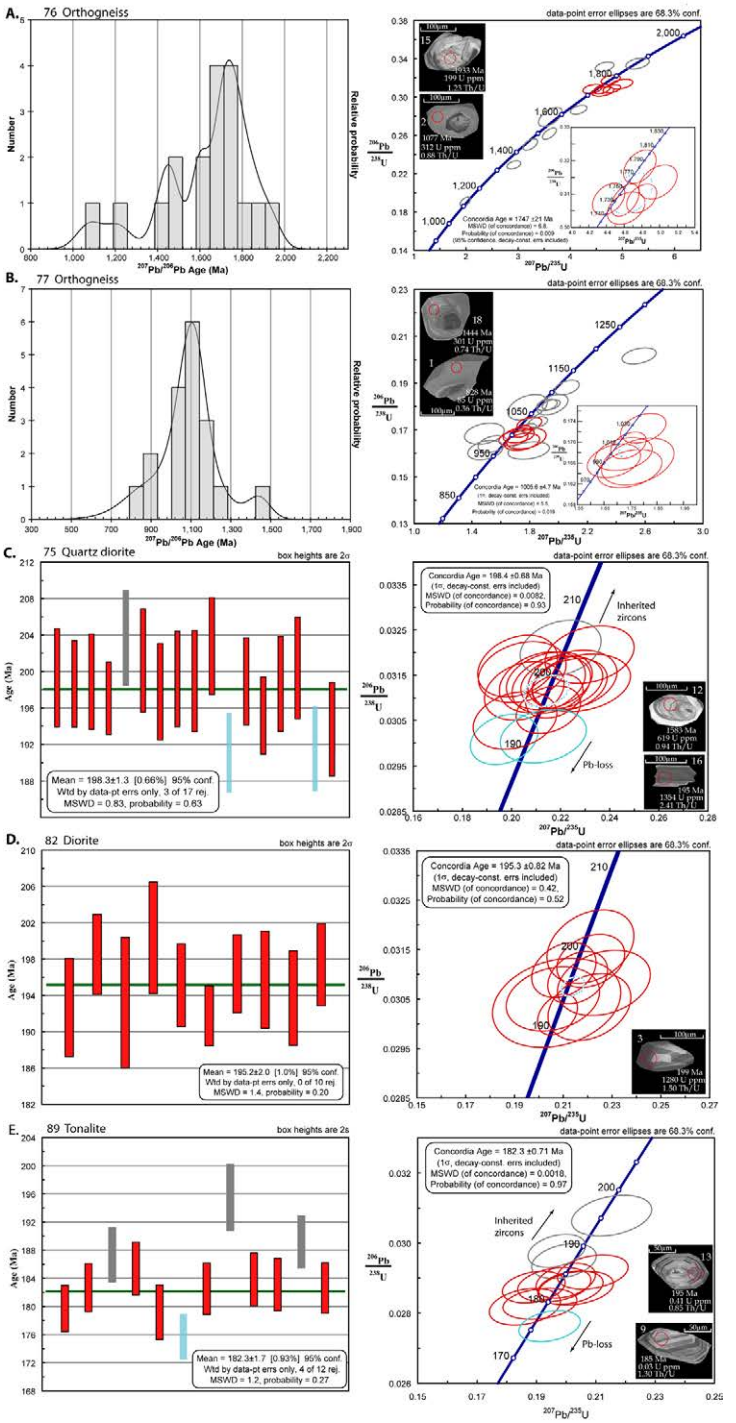

FIG. 4. U-Pb ages for samples from rocks associated with gold-bearing quartz veins at Copacabana mining distric. Ages are calculated based on the Concordia diagrams and weighted mean $^{206}Pb/^{238}U$ ages histograms. Furthermore, ages distribution for metamorphic zircons (A and B) and Concordia diagram are shown, and for each sample one or more representative analyzed zircons. Histogram diagrams are also shown the distribution for Pb loss (sky-blue bars), and inheritance (gray color) in some of the analyzed zircons (C and E). **A.** 76: orthogneiss and **B.** 77: orthogneiss, both samples from Arequipa Massif. **C.** 75: quartz diorites and **D.** 82: diorite, both samples from Coastal Batholith (Punta Coles Super-unit). **E.** 89: tonalite from Coastal Batholith (Zafranal Super-unit).

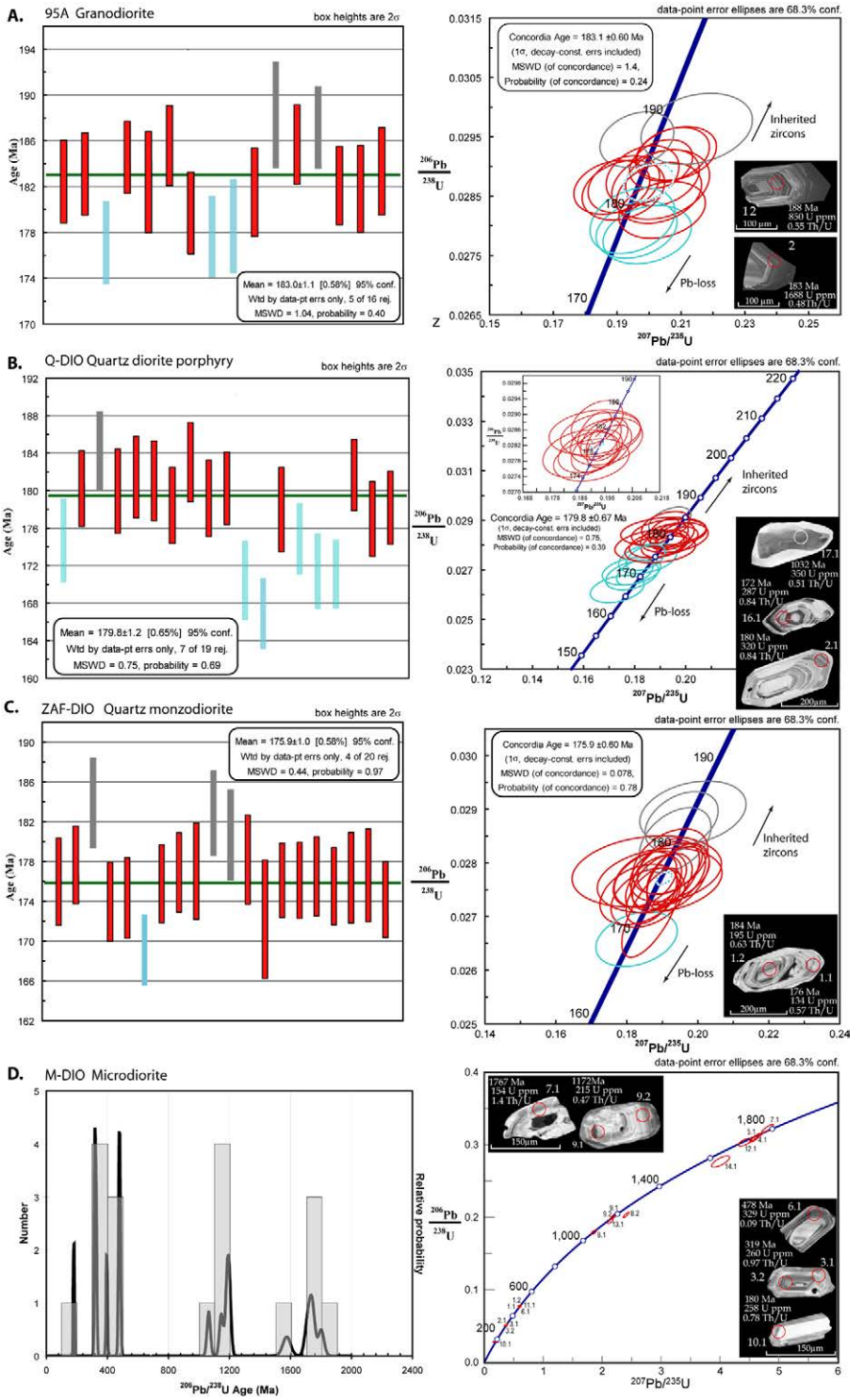

FIG. 5. U-Pb ages for rock samples from the Zafranal porphyry. Ages are calculated based on the Concordia diagrams and weighted mean $^{206}Pb/^{238}U$ ages histograms. Furthermore, in histogram diagrams are also shown the distribution for Pb loss (sky-blue bars), and inheritance (gray bars) in some of the analyzed zircons (A, B, and C). **A.** 95A: granodiorite; **B.** Q-DIO: quartz diorite porphyry; **C.** ZAF-DIO: quartz monzodiorite and **D.** M-DIO: microdiorite. All samples from Coastal Batholith (Zafranal Super-unit).

Inter-mineral porphyry 1. The Zafranal quartz-monzodiorite porphyry (ZAF-DIO) from approximately 1 km east of the center of the main orebody (Fig. 3) pervasively hydrothermally altered and mineralized. The zircons from this sample are elongate to sub-round in shape and less than 300 μm in length. CL images mainly show strong oscillatory zoning and irregular zoning. Other zircons display small relict cores, which are elongate euhedral prisms with oscillatory zoning surrounded by rim with resorption features. Rims show different orientation oscillatory zoning and are large enough to be analyzed (5C). Twenty-one points were analyzed including rims and cores. Three cores yielded U-Pb ages between 180-184 Ma, which are interpreted as the inherited zircons from the precursor pluton granodiorite (sample 95A). The analyzed rims yielded U-Pb age of 176 Ma, very close to age established by the remaining sixteen zircons (175.9 Ma). One of the crystal give an age slightly younger (169 Ma). We interpret the statistically more robust and age of 175.9±1.0 Ma to more accurately reflect the crystallization age for quartz-monzodiorite porphyry.

Inter-mineral porphyry 2. The microdiorite (M-DIO) forms a second porphyry copper-related, from approximately 0.5 km from east part of the main porphyry body (Fig. 3). Microdiorite cut the Zafranal quartz-monzodiorite porphyry, and is characterized by showing a pervasive hydrothermal alteration, mineralization and dynamic metamorphism features. Zircons are elongate to sub-rounded (less than 150 μm in length), subhedral in shape. The CL images reveal a varied internal structure and features (Fig. 5D). Some grains display small cores surrounded with mantle weak oscillatory zoning. Also commonly show crystals with prominent oscillatory zoning. Eighteen spots were analyzed on fourteen zircon grains, included rim and core. The cores do not show substantial variation in isotopic measurements in relation to the rims. The older population of zircons have a late Paleproterozoic $^{206}Pb/^{238}U$ age of 1801-1710 Ma (four crystal zircons), whereas other zircons with more homogeneous rim area has a Mesoproterozoic $^{206}Pb/^{238}U$ age of 1575-1064 Ma (six crystal zircons). The other younger population of zircons with a marked oscillatory zoning. Three crystal zircons have an Ordovician (478-481 Ma) U-Pb age. Four analyzed in three zircons have Devonian-Carboniferous U-Pb age of 396-319 Ma. Furthermore, one zircon yield an age of 179.7 ± 3 Ma (Fig. 5D), and therefore is interpreted as maximum crystallization age of the microdiorite.

6.3 Late Jurassic

Late intrusion. At Huano village, a granular tonalite (86, Torrecillas Super-unit). The zircons from this sample are slightly elongate to sub-round (less than 120 μm in length), subhedral in shape. CL image show, some crystal highlights very high concentrations of U in the crystal center, more moderate values in an intermediate shell and high concentrations in the rim. Twenty spots were analyzed including center and rim of zircons. Nine crystal center yielded U-Pb ages between 140-144 Ma, with very high U concentrations of 2481-1000 ppm and also high Th/U values of center (0.8-1.57). Eleven rims yielded U-Pb ages in 149-146 Ma, with U concentrations of 875-513 ppm and Th/U values between 0.61-0.94. If the less concordant analyses are excluded, the rest plot yielded a zircon U-Pb age of 145.9±1.4 Ma (Fig. 6).

7. Discussion

Four views emerge from the data obtained: **1.** Arequipa Massif, **2.** Early Jurassic arc extent of the Coastal Batholith, **3.** Intrusive bodies associated with ore mineralization in the quartz veins and Zafranal porphyry deposit, and **4.** late Jurassic magmatic pulse.

7.1. Arequipa Massif

Arequipa Massif includes rocks displaying protolith ages of 1.9 Ga (Dalmayrac *et al.*, 1977; Cobbing *et al.*, 1977) and other rocks showing Mesoproterozoic protolith and metamorphism ages of 1.2-1.0 Ga (Wasteneys *et al.*, 1995; Loewy *et al.*, 2004). Along the Cincha-Lluta Fault System, the metamorphic rocks are thrusted over the Mesozoic series of the Western Peruvian Mesozoic Basin (Caldas, 1993; Carlotto *et al.*, 2008, Fig. 1). The Arequipa Massif in this area contains Paleoproterozoic zircons (samples 76 and 77) and core zircons with rims plot on discordia resulting from Pb-loss during Grenvillian metamorphism (Fig. 4A, B), similar to migmatitic gneisses of the Camaná-Mollendo domain, described by Casquet *et al.* (2010). This confirms the Arequipa Massif extent to the western flank of the Western Cordillera.

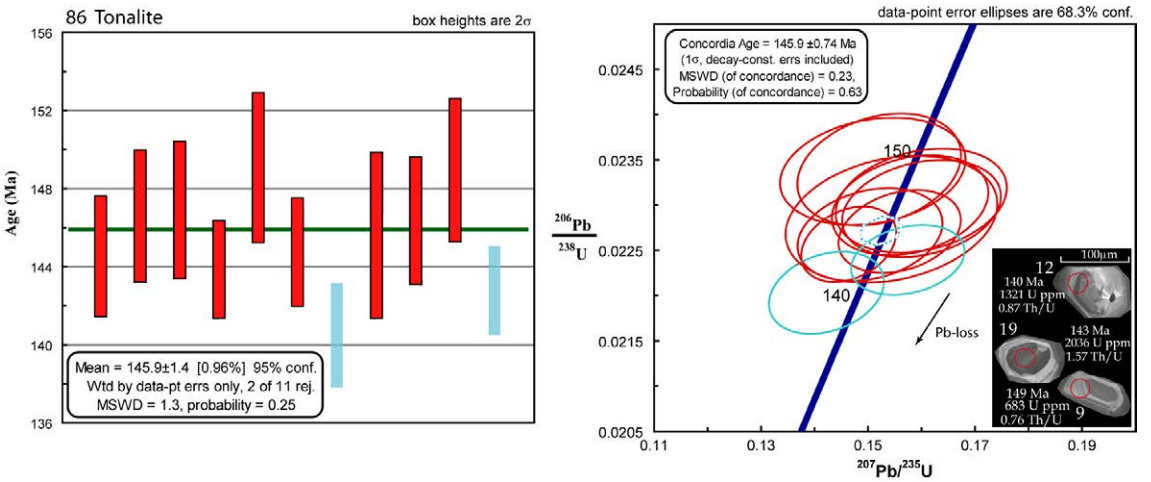

FIG. 6. U-Pb ages for rock samples from the Zafranal porphyry. Ages are calculated based on the Concordia diagrams and weighted mean $^{206}Pb/^{238}U$ ages histograms. Furthermore, in concordia diagram is also shown representative analyzed zircons, and in histogram diagram is shown the distribution for Pb loss (sky-blue bars) in two of the analyzed zircon. (86) Tonalite from Coastal Batholith (Torrecillas Super-unit).

7.2. Early Jurassic arc extent of the Coastal Batholith

The U-Pb ages reported herein of mafic and felsic intrusive rocks from Chuquibamba to Arequipa in southern Peru (Fig. 1, Coastal Batholith), shows that first magmatic activities occurred during 200-174 Ma.

For the magmatic belt in the study area (Fig. 1) Cordani *et al.* (1985) indicated an early Jurassic K-Ar ages (189±11 Ma), which is considered as the minimum age of the tectonomagmatic process. Later, Mukasa (1986) published two early Jurassic U-Pb ages (188 and 184 Ma) from northwest of Arequipa. He indicated that these rocks represent the plutonic substructure of a Jurassic continental arc of unknown extent. In the south of Arequipa, Demouy *et al.* (2012) got new U-Pb ages for gabbros-diorites, which restricted early Jurassic age (200-175 Ma) to a mafic magmatism (Fig. 1). Our results show that the first magmatic activity in this study area occurred during 198.3-195.2 Ma (Sinemurian; Fig. 4C, D), and is associated with diorite-quartz diorite rocks of Punta Coles Super-unit (Table 1). A second magmatic phase encloses tonalite-granodiorite rocks (Table 1) emplaced at 183.0-175.9 Ma (Pliensbachian-Toarcian; Figs. 4E and 5) of Zafranal Super-unit. The second magmatic phase include small microdiorites, quartz diorites and quartz monzodiorite porphyritic stocks and dikes (Table 1) with an EW-trend at 179.8-175.9 Ma (Fig. 5B, C). The two magmatic suites make up a thin magmatic belt (15x130 km) that extends from southern Chuquibamba to the southern Arequipa (Fig. 1) .

7.3. Intrusive associated with gold-bearing quartz veins and Zafranal porphyry deposit

7.3.1. Gold-bearing quartz vein mineralization

The gold-bearing quartz vein systems in Copacabana and Rinconada de Chapi mining districts have metamorphic and volcano-sedimentary host rocks, respectively. Early diorites (198.3-195.2 Ma; Fig. 2) of Punta Coles Super-unit intruded the metamorphic host rocks of the gold-bearing quartz veins and restrict their extent (Cerro Gandolfo, Fig. 2). Therefore it is inferred that the gold-bearing quartz veins were formed before *ca.* 198.3 Ma.

7.3.2. Zafranal porphyry deposit

The first radiometric ages for the Zafranal porphyry copper deposit were published by Rivera (2012a), who reported $^{40}Ar/^{39}Ar$ plateau ages for hydrothermal biotite of 82.41±0.43 Ma from Zafranal diorite and 83.37±0.54 and 81.16±0.43 Ma from microdiorite. According to this author, the Zafranal diorite and microdiorite are associated with copper mineralization, and he concluded that the alteration and mineralization developed in the late

Cretaceous. However, the $^{40}Ar/^{39}Ar$ ages for Zafranal hydrothermal biotites only record cooling under 320±30°C; biotite closure temperature estimated using Dodson (1973) and parameters presented by Harrison *et al.* (1985) and McDougall and Harrison (1999). Whether this thermal event was related or not to the hydrothermal copper mineralization of Zafranal is considered uncertain here, as no other, isotopic data are available for constraint ore formation. While, the use of Zircon U-Pb dating from intrusions associated with porphyry copper mineralization makes possible to us confidently assign crystallization ages to the various intrusive units, as zircon has the highest known closure temperature for Pb diffusion, which exceeds 900°C for zircons of typical sizes (Cherniak and Watson, 2000, and references therein). At Zafranal, three phases of porphyry intrusions were dated by U-Pb, with the oldest being the granodiorite precursor batholith at 183.0±1.1 Ma. The second phase is a quartz diorite intrusion at 179.8±1.2 Ma, and the third phase is a quartz monzodiorite at 175.9±1.0 Ma (Fig. 7). As the multiphase porphyry complex at Zafranal is hosting a copper mineralized stockwork, we postulate that copper mineralization also was introduced during the early Jurassic, while the late Cretaceous $^{40}Ar/^{39}Ar$ biotite ages of Rivera (2012a) represent a thermal overprint, which could be either a late hydrothermal activity or just heating by Cretaceous magmatic processes of the Arequipa Segment of Coastal Batholith of Peru (*i.e.*, Demouy *et al.*, 2012).

7.3.3. Late Jurassic

Cordani *et al.* (1985) reported a K-Ar age of late Jurassic intrusion east of the CLFS (157±14 Ma). Later Demouy *et al.* (2012) published a late Jurassic age (U-Pb, 154.7±1.0 Ma) for a monzonite sill from the south of Arequipa, which is associated with sedimentary formations without any presence of magmatic activity between 160.5 to 90 Ma. However, our data set combined with the recently published U-Pb ages (Santos *et al.*, 2016), show that two late Jurassic magmatic events developed west of the CLFS, and cover a wide area west of Chuquibamba (Fig. 1). First magmatic activity occurred during 158-157 Ma (Oxfordian), containing biotite-rich granodiorite and granite-monzogranite rocks of Tembladera and Chillihuay units, respectively. A second magmatic phase encloses amphibole-rich tonalite rocks emplaced at 145.9 Ma (Tithonian) of Torrecillas Super-unit. Both magmatic events probably ended with injection of copper mineralizing fluid (*e.g.,* Tinajas prospect 152 Ma and Campanero prospect 141 Ma, Fig. 1).

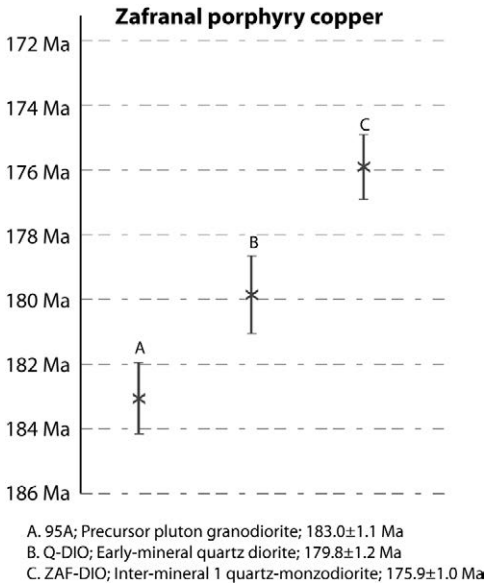

FIG. 7. Summary of magmatic ages determined at Zafranal porphyry copper based on weighted mean averages of ^{207}Pb-corrected $^{206}Pb/^{238}U$ spot ages using SHRIMP and LA-ICP-MS. Errors shown at 2σ levels.

Overall, our geochronology data coincide with the first magmatic pulse from 200-175 Ma previously identified in the southern sector of the Arequipa Segment of the Coastal Batholith of Peru by Demouy *et al.* (2012). Later the early Jurassic arc was overprint by felsic Cretaceous intrusive bodies (90-60 Ma, Demouy *et al.*, 2012), hence the biotites of some early Jurassic rocks register the thermal overprint of these two main magmatic pulses (*e.g.,* Zafranal porphyry copper).

8. Conclusions

Outcrops of metamorphic rocks in Western Cordillera (Western Peruvian Mesozoic Basin) correspond to Arequipa Massif with Paleoproterozoic igneous protolith and Mesoproterozoic Grenville-age metamorphism (1.75 Ga and 1 Ga).

The Coastal Batholith exposed in the study area, along the fault-bounded thin magmatic belt (<15 km wide) was emplaced into Arequipa Massif during the early Jurassic. Two main magmatic events are identified: (**1**) Early mafic magmatic event from *ca.* 200-194 Ma that correspond to the Punta Coles Super-unit (200-188 Ma). It consists mainly of diorites and quartz diorites, and (**2**) A second event of dominantly felsic magmatism from *ca.* 184-175 Ma that corresponds to the Zafranal Super-unit (188-176 Ma). The porphyritic stocks with copper mineralization at Zafranal crystallized from 181 to 175 Ma and provide a maximum age for the hydrothermal processes.

Late Jurassic magmatic events comprised of granodiorites and granitic-monzogranitic bodies emplaced from 158 to 157 Ma, which correspond to Tembladera and Chillihuay units. A late magmatic phase encloses tonalite plutonics emplaced at *ca.* 145.9 Ma, corresponding to Torrecillas Super-unit (150-145 Ma).

Mineralizing processes in this area occurred in the early Jurassic. Gold-bearing quartz vein mineralization formed in early stages of the Coastal batholith (>200 Ma), while copper minerals in the Zafranal porphyritic host rocks may have been introduced from 181.1 to 174.7 Ma. A late Cretaceous thermal event registered by biotite with $^{40}Ar/^{39}Ar$ age from 83 to 81 Ma (previously considered as the mineralizing event) constitutes just a thermal, overprint, which could be either a late hydrothermal alteration or a local heating from an unidentified magmatic source. Overall, much of copper mineralization in this area is thought to be linked to the last stages of each magmatic suite (*e.g.,* Zafranal, Tinajas and Campanero).

Acknowledgments

We wish to express our gratitude to INGEMMET and AQM Peru Copper S.A.C. for the support in the logistics of obtaining the Coastal Batholith samples and information generated during their exploration stages in the Zafranal cluster. John Cervantes and Paola LLamoca of Regional Geology from Geological Survey of Peru (INGEMMET) have greatly helped with this project. This work is part of the master thesis of the first author, with the support of the high-resolution geochronology laboratory of the Institute of Geosciences of the University of Sao Paulo-Brazil and Laboratory of China University of Geosciences (Wuhan).

References

Acosta, J.; Sempere, T. 2017. Evolución tectónica y metalogénesis del Perú. *In* Congreso Internacional de Prospectores y Exploradores, No. 10, Instituto de Ingenieros de Minas del Perú, Abstract: 2-7. Lima.

Allmendinger, R.W.; Jordan, T.E.; Kay, S.M.; Isacks, B.L. 1997. The evolution of the Altiplano-Puna plateau of the Central Andes. Annual Review of Earth and Planetary Sciences 25: 139-174.

Atherton, M.; Pitcher, W.; Warden, V. 1983. The Mesozoic marginal basin of central Peru. Nature 305: 303-305.

Atherton, M.; Warden, V.; Sanderson, L.M. 1985. The Mesozoic marginal basin of central Peru: A geochemical study of within plate-edge volcanism. *In* Magmatism at a plate edge: The Peruvian Andes: Glasgow, Blackie (Pitcher, W.S.; Atherton, M.P.; Cobbing, E.J.; Beckinsale, R.D.; editors). John Wiley and Sons: 47-58.

Bahlburg, H.; Carlotto, V.; Cárdenas, J. 2006. Evidence of Early to Middle Ordovician arc volcanism in the Cordillera Oriental and Altiplano of southern Peru, Ollantaytambo Formation and Umachiri beds. Journal of South American Earth Sciences 22: 52-65.

Beckinsale, R.D.; Sánchez, A.; Brook, M.; Cobbing, E.J.; Taylor, W.P.; Moore, N.D. 1985. Rb-Sr wholerock isochron and K-Ar age determinations for the Coastal Batholith of Peru. *In* Magmatism at a plate edge: the Peruvian Andes (Pitcher, M.P.; Cobbing, E.J.; Beckinsale, R.D.; editors). Blackie Halsted: 177-202. London.

Benavides, V. 1956. Cretaceous system in northern Peru. Bulletin of American Natural History 108: 252-494.

Benavides, V. 1962. Estratigrafía Pre-terciaria de la región de Arequipa. *In* Congreso Nacional de Geología, No. 2. Boletín de la Sociedad Geológica del Perú 38: 5-63. Lima.

Benavides. V. 1999. Orogenic evolution of the Peruvian Andes: The Andean cycle. Special Publication 7: 61-107.

Boeckhout, F. 2012. Geochronological constraints on the Paleozoic to early Mesozoic geodynamic evolution of southern coastal Peru. Ph.D. Thesis (Unpublished). University Genève: 176 p.

Boily, M.; Brooks, C.; Ludden, J.N. 1989. Chemical and isotopic evolution of the Coastal Batholith of southern Peru. Journal of Geophysical Research 94: 483-498.

Caldas, J. 1993. Geología de los cuadrángulos de Huambo y Orcopampa (Hojas 32r y 31r). Instituto Geológico Minero y Metalúrgico, Boletín Serie A: 62 p. Lima.

Camus, F. 2003. Geología de los sistemas porfíricos en los Andes de Chile. Servicio Nacional de Geología y Minería: 267 p.

Carlotto, V.; Cárdenas, J.; Carlier, G. 2008. The lithosphere of Southern Peru: A result of the accretion of allochthonous blocks during the Mesoproterozoic. *In* International Symposium on Andean Geodynamics, No. 7, Extended Abstract: 105-108.

Carlotto, V.; Quispe, J.; Acosta, H.; Rodríguez, R.; Romero, D.; Cerpa, L.; Mamani, M.; Díaz, E.; Navarro, P.; Jaimes, F.; Velarde, T.; Lu, S.; Cueva, E. 2009a. Dominios geotectónicos y Metalogénesis del Perú. Boletín de la Sociedad Geológica del Perú 103: 1-89.

Carlotto, V.; Rodríguez, R.; Acosta, H.; Cárdenas, J.; Jaillard, E. 2009b. Alto estructural Totos-Paras (Ayacucho): límite paleogeográfico en la evolución mesozoica de las cuencas Pucará (Triásico superior-Liásico) y Arequipa (Jurásico-Cretácico). Boletín de la Sociedad Geológica de Perú, Volumen especial Víctor Benavides Cáceres 7: 1-46.

Casquet, C.; Fanning, C.; Galindo, C.; Pankhurst, R.; Rapela, C.; Torres, P. 2010. The Arequipa Massif of Peru: new SHRIMP and isotope constraints on a Paleoproterozoic inlier in the Grenvillian orogeny. Journal of South American Earth Science 29: 128-142.

Cherniak, D.J.; Watson, E.B. 2000. Pb diffusion in zircon. Chemical Geology 172: 5-24.

Chew, D.M.; Schaltegger, U.; Kosler, J.; Whitehouse, M.J.; Gutjahr, M.; Spikings, R.A.; Miskovic, A. 2007. U-Pb geochronologic evidence for the evolution of the Gondwanan margin of the north-central Andes. Geological Society of America Bulletin 119 (5): 697-711.

Chew, D.M.; Magna, T.; Kirkland, C.L.; Miskovic, A.; Cardona, A.; Spikings, R.; Schaltegger, U. 2008. Detrital zircon fingerprint of the Proto-Andes: evidence for a Neoproterozoic active margin? Precambrian Research167 (1-2): 186-200.

Clark, A.H. 1993. Are outsize porphyry copper deposits either anatomically or environmentally distinctive? Society of Economic Geologists Special Publication 2: 213-282.

Clark, A.H.; Farrar, E.; Kontak, D.J.; Langridge, R.J.; Arenas, F.; M.J., France, L.J.; McBride, S.L.; Woodman, P.L.; Wasteneys, H.A.; Sandeman, H.A.; Archibald, D.A. 1990a. Geologic and geochronologic constraints on the metallogenic evolution of the Andes of southeastern Peru. Economic Geology 85: 1520-1583.

Clark, A.H.; Tosdal, R.M.; Farrar, E.; Plazolles, V.A. 1990b. Geomorphologic environment and age of supergene enrichment of the Cuajone, Quellaveco, and Toquepala porphyry copper deposits, southeastern Peru. Economic Geology 85: 1604-1628.

Cobbing, E.J.; Pitcher, W.S. 1972. Plate tectonics and the Peruvian Andes. Nature 246: 51-53.

Cobbing, E.J.; Pitcher, W.S.; Taylor, W.P. 1977. Segments and super-units in the Coastal Batholith of Peru. Journal of Geology 85: 625-631.

Coira, B.; Davidson, J.; Mpodozis, C.; Ramos, V. 1982. Tectonic and magmatic evolution of the Andes of northern Argentina and Chile: Earth Science Reviews 18: 302-332.

Cordani, U.G.; Kawashita, K.; Siegl, G.G.; Vicente, J.C. 1985. Geochronological results from the southeastern part of the Arequipa massif. Comunicaciones 35: 45-51.

Couch, R.; Whitsett, R.; Huehn, B.; Briceno-Guadalupe, L. 1981. Structures of the continental margin of Peru and Chile. Geological Society of America 154: 703-726.

Dalmayrac, B.; Lancelot, J.R.; Leyreloup, A. 1977. Two-billion-year granulites in the Late Precambrian metamorphic basement along the Southern Peruvian coast. Science 198: 49-51.

Davidson, J.; Mpodozis, C. 1991. Regional geologic setting of epithermal gold deposits, Chile. Economic Geology 86: 1174-1186.

De Ruijter, M.A.; Mosher, G.Z.; Ghaffari, H.; Danon-Schaffer, M.; Hafez, S.A.; Guzman, C.; Muir, W. 2013. Technical report and preliminary assessment of the Zafranal project, Peru. AQM Copper Inc.: 256 p.

Demouy, S.; Paquette, J.; De Saint Blanquat, M.; Benoit, M.; Belousova, E.; O´Reilly, S.; Garcia, F.; Tejada, L.; Gallegos, R.; Sempere, T. 2012. Spatial and temporal evolution of liassic to Paleocene arc activity in Southern

Peru un raveled by zircon U-Pb and Hf *in situ* data on plutonic rocks. Lithos 155: 183-200.

Dodson, M.H. 1973. Closure temperature in cooling geochronological and petrological systems. Contributions to Mineralogy and Petrology 40: 259-274.

Fernandez-Baca, A. 2011. El pórfido de cobre-oro Zafranal. *In* Congreso Internacional de Prospectores y Exploradores, No. 7, Abstract, CD-ROM: 4 p. Lima.

Gustafson, L.B.; Hunt, J.P. 1975. The porphyry copper deposit at El Salvador, Chile. Economic Geology 70: 857-912. doi: 10.2113/gsecongeo.70.5.857.

Harrison, T.M.; Duncan, I.; McDougall, I. 1985. Diffusion of ^{40}Ar in biotite: temperature, pressure and compositional effects. Geochimica et Cosmochimica, Acta 49: 2461-2468.

Hoskin, P.W.O.; Schaltegger, U. 2003. The Composition of Zircon and Igneous and Metamorphic Petrogenesis. Reviews in Mineralogy and Geochemistry 53: 27-62.

Huamán, C.; Bustamante, J.; Gálvez, S. 2014. Mineralización supérgena del pórfido Cu-Au-Mo, Proyecto Ocaña, Arequipa-Perú. *In* Congreso Peruano de Geología, No. 17, Resúmenes extendidos: 4 p. Lima.

INGEMMET. 2001. Mapa Geológico del cuadrángulo de Chuquibamba, scale 1:100 000, Lima.

Isacks, B.L. 1988. Uplift of the central Andean plateau and bending of the Bolivian orocline. Journal of Geophysical Research 93: 3211-3231.

Jacay, J.; Semperé, T.; Husson, L.; Pino, A. 2002. Structural characteristics of the Incapuquio Fault System, southern Peru. *In* International Symposium on Andean Geodynamics, No. 5, Extended Abstracts: 319-321. Toulouse.

Jaillard, E. 1992. La fase peruana (Cretácico superior) en la margen peruana. Boletín de la Sociedad Geológica del Perú 83: 81-87.

James, D.E. 1971. Plate Tectonic Model for the Evolution of the Central Andes. Geological Society of America Bulletin 82: 3325-3346.

Jenks, W.F.; Harris, E.G. 1953. Plutonics near Arequipa as a petrologic sample of the Coastal Batholith in Peru. Boletín de la Sociedad Geológica del Perú 26: 79-94.

JICA (Japan International Cooperation Agency). 1986. Report on mineral exploration in Cotahuasi area, Republic Peru. Phase I. Metal Minig Agency of Japan: 223 p.

Kretz, R. 1983. Symbols for rock-forming minerals. American Mineralogist 68: 277-279.

Liu, Y. 2011. Guide Book for ICPMSDataCal. China University of Geosciences, China. State Key Laboratory of Geological Processes and Mineral Resources: 32 p.

Loewy, S.L.; Connelly, J.N.; Dalziel, I.W. 2004. An orphaned block: The Arequipa-Antofalla basement of the Central Andean margin of South America. Geological Society of America Bulletin 116: 171-187.

Lowell, J.D.; Guilbert, J.M. 1970. Lateral and vertical alteration-mineralization zoning in porphyry ore deposits: Economic Geology 65: 373-408.

Ludwig, K.R. 2001. User´s manual for Isoplot/ex Version 2.49. A Geochronological Toolkit for Microsoft Excel. Berkeley Geochronological Center, Special Publication 1a: 1-55.

Martínez, W.; Cervantes, J. 2003. Rocas ígneas en el sur del Perú: nuevos datos geocronométricos, geoquímicos y estructurales entre los paralelos 16° y 18°30' S. Boletín del Instituto Geológico Minero y Metalúrgico (INGEMMET) 26, Serie D (Estudios Regionales): 140 p. Lima.

McDougall, I.; Harrison, T.M. 1999. Geochronology and Thermochronology by the $^{40}Ar/^{39}Ar$ Method. Oxford University Press: 269 p. New York.

Mukasa, S.B. 1986. Zircon U-Pb ages of super-units in the Coastal batholith, Peru: Implications for magmatic and tectonic processes. Geological Society of America Bulletin 97: 241-254.

Mukasa, S.B.; Henry, D.J. 1990. The San Nicolas batholith of coastal Peru: early Palaeozoic continental arc or continental rift magmatism? Journal of the Geological Society 147: 27-39.

Noury, M.; Philippon, M.; Bernet, M.; Paquette, J-L.; Sempere, T. 2017. Geological record of flat slab-induced extension in the southern Peruvian forearc. Geological Society of America 45: 723-726.

Oncken, O.; Hindle, D.; Kley, J.; Elger, K.; Victor, P.; Schemmann, K. 2006. Deformation of the Central Andean upper plate system-Facts, Fiction, and constrains for the plateau models. *In* The Andes, Active Subduction Orogeny (Oncken, O.; Franz, G.; Giese, P.; Götze, H.; Ramos, V.; Strecker, M.; Wigger, P.; editors). Springer-Verlag Berlin Heidelberg: 1-27.

Perelló, J.; Carlotto, V.; Zárate, A.; Ramos, P.; Posso, H.; Neyra, C.; Caballero, A.; Fuster, N.; Muhr, R. 2003. Porphyry-style alteration and mineralization of the middle Eocene to early Oligocene Andahuaylas-Yauri belt, Cuzco region, Peru. Economic Geology 98: 1575-1605.

Petford, N.; Atherton, M. 2003. Rifting, insertical magmatism and continental arc construction, Peru. American Geophysical Union, Fall Meeting, Abstract: V41A-04.

Pitcher, W.S. 1985. A multiple and composite batholith. *In* Magmatism at a plate edge: The Peruvian Andes

(Pitcher, M.P.; Cobbing, E.J.; Beckinsale, R.D.; editors). Blackie Halsted, London: 93-101.

Quang, C.X.; Clark, A.H.; Lee, J.K.W.; Guillén B.J. 2003: $^{40}Ar/^{39}Ar$ ages of hypogene and supergene mineralization in the Cerro Verde-Santa Rosa porphyry Cu-Mo cluster, Arequipa, Peru. Economic Geology 98: 1683-1696.

Quang, C.X.; Clark, A.H.; Lee, J.K.W. 2005. Response of Supergene processes to Episodic Cenozoic uplift, pediment erosion, and ignimbrite eruption in the porphyry copper province of southern Peru. Economic Geology 100: 87-114.

Ramos, V.A. 2008. The basement of the Central Andes: the Arequipa and related terranes. Annual Review of Earth and Planetary Sciences 36: 289-324.

Ramos, V.A.; Aleman, A. 2000. Tectonic Evolution of the Andes (Cordani, U.G.; Milani, E.J.; Thomaz Filho, A.; Campos, D.A; editors). *In* Tectonic Evolution of South America. International Geological Congress, No. 31, Special Publication: 635-685. Rio de Janeiro.

Reitsma, M.J. 2012. Reconstructing the Late Paleozoic: Early Mesozoic plutonic and sedimentary record of south-east Peru: Orphaned back-arcs along the western margin of Gondwana. Ph.D. Thesis (Unpublished). Université de Genève: 246 p.

Rivera, F.; Moretti, A.; Baumgartner, R. 2008. La franja Cretácea de pórfidos de cobre en el sur del Perú. *In* Congreso Peruano de Geología, No. 14. Resúmenes extendidos: 6 p. Lima.

Rivera, F.; León, J.; Cano, O.; Huamán, M. 2010. Controles de mineralización en el pórfido de Cu Zafranal, en el sur de Perú. *In* Congreso Peruano de Geología, No. 1, Resúmenes extendidos: 4 p. Lima.

Rivera, F. 2012a. Geología y geocronología del pórfido de Cu-Au Zafranal, en el sur del Perú. *In* Congreso Peruano de Geología, No. 16, Resúmenes extendidos: 6 p. Lima.

Rivera, F. 2012b. Nuevos Datos Geocronológicos en la Franja Cretácea de Pórfidos de Cobre en el Sur del Perú. Sociedad Geológica del Perú, Boletín 106: 49-57.

Romero, D.; Ticona, P. 2003. Memoria descriptiva de la revisión y actualización del cuadrángulo de Huambo (Hoja 32r), Instituto Geológico Minero y Metalúrgico: 28 p. Lima, Perú.

Roperch, P.; Sempere, T.; Macedo, O.; Arriagada, C.; Fornari, M.; Tapia, C.; García, M.; Laj, C. 2006. Counterclockwise rotation of late Eocene-Oligocene forearc deposits in southern Peru and its significance for oroclinal bending in the central Andes. Tectonics, American Geophysical Union (AGU) 25 (3): TC3010.

Sandeman, H.A.; Clark, A.H.; Farrar, E. 1995. An integrated tectonomagmatic model for the evolution of the southern Peruvian Andes (13-20°S) since 55 Ma. International Geology Review 37: 1039-1073.

Santos, A.; Weimin, G.; Tassinari, C.; Soberon, D.; Ccallo, W. 2016. Geocronología U-Pb sobre zircones en la contrastación de la evolución espacial-temporal del magmatismo y la metalogenia del Batolito de la Costa "segmento Arequipa". *In* Congreso Peruano de Geología, No. 18. Resúmenes extendidos: 4 p. Lima.

Sato, K.; Tassinari, C.C.G.; Basei, M.A.S.; Siga, J.O.; Onoe, A.T.; De Souza, M.D. 2014. Sensitive High-Resolution Ion Microprobe (SHRIMP IIe/MC) of the Institute of Geosciences of the University of Sao Paulo, Brazil. Geologia USP. Série Científica 14 (3): 3-18.

Schildgen, T.; Ehlers, T.; Whipp, D.; Van Soest, M.; Whipple, K.; Hodges, K. 2009. Quantifying canyon incision and Andean Plateau surface uplift, southwest Peru: a thermochronometer and numerical modeling approach. Journal of Geophysical Research 114: 1-22.

Seedorff, E.; Dilles, J.H.; Proffett, J.M.; Einaudi, M.T.; Zurcher, L.; Stavast, W.J.A.; Johnson, D.A.; Barton, M.D. 2005. Porphyry deposits: Characteristics and origin of hypogene features. Economic Geology Anniversary 100: 251-298.

Shackleton, R.M.; Ries, A.C.; Coward, M.P.; Cobbold, P.R. 1979. Structure, metamorphism and geochronology of the Arequipa massif of Coastal Peru. Journal of the Geological Society 136: 195-214. London. doi: 10.1144/gsjgs.136.2.0195.

Siivola, J.; Schmid, R. 2007. List of mineral abbreviation. *In* Metamorphic Rocks. A Classification and Glossary of Terms. Cambridge University Press: 93-110.

Sillitoe, R.H.; Thompson, F.H. 1998. Intrusion-Related Vein Gold Deposits: Types, Tectono-Magmatic Settings and Difficulties of Distinction from Orogenic Gold Deposits: Resource Geology 48: 237-250.

Sillitoe, R.H.; Perelló, J. 2005. Andean Copper Province: Tectonomagmatic Setting, Deposit Types, Metallogeny, Exploration and Discovery. Economic Geology, Anniversary 100: 845-890.

Sillitoe, R.H. 2010. Porphyry Copper System. Economic Geology 105: 3-41. doi: 10.2113/gsecongeo.105.1.3.

Sillitoe, R.H. 2003. Iron oxide-copper-gold deposits an Andean view. Mineralium Deposita 38: 787-812.

Simmons, A.T.; Tosdal, R.M.; Wooden, J.L.; Mattos, R.; Concha, O.; McCracken, S.; Beale, T. 2013. Punctuated magmatism associated with porphyry Cu-Mo formation in the Paleocene to Eocene of Southern Peru: Economic Geology 108: 625-639.

Sobolev, S.V.; Babeyko, A.Y. 2005. What drives orogeny in the Andes? Geological Society of America Bulletin 33 (8): 617-620.

Stewart, J.W.; Evernden, J.F.; Snelling, N.J. 1974. Age determinations from Andean Peru: a reconnaissance survey. Geological Society of America Bulletin 85: 1107-1116.

Streckeisen, A.L. 1973. Plutonic rocks: Classification and Nomeclature Recommended by the I.U.G.S. Subcommission on the Systematics of Igneous. Rocks, Geotimes 18: 26-30.

Tejada, W. 2010. The Zafranal Cu Discovery. *In* Congreso Internacional de Prospectores y Exploradores, No. 6, Abstract CD-ROM: 2 p.

Thorpe, R.S. 1984. The tectonic setting of active Andean volcanism: *In* Andean Magmatism (Harmon, R.S.; Barreiro, B.A.; editors). Birkhäuser Boston: 4-8.

Tosdal, R.M.; Farrar, E.; Clark, A. 1981. K-Ar geochronology of the late Cenozoic volcanic rocks of the Cordillera Occidental, southernmost Peru. Journal of Volcanology and Geothermal Research 10 (1-3): 157-173. doi: 10.1016/0377-0273(81)90060-3.

Tosdal, R.M.; Clark, A.H.; Farrar, E. 1984. Cenozoic polyphase landscape and tectonic evolution of the Cordilleran Occidental, southernmost Peru: Geological Society of America Bulletin 95: 1318-1332.

Vargas, L. 1970. Geología del Cuadrángulo de Arequipa (Hoja 33s). Servicio de Geología y Minería de Perú (actualmente el Instituto Geológico Minero y Metalúrgico (INGEMMET), Carta Geológica Nacional 24, Serie A: 64 p.

Vicente, J.C.; Sequeiros, F.; Valdivia, S.; Zavala, J. 1979. El sobre-escurrimiento de Cincha-Lluta: element del accidente mayor Andino al NW de Arequipa. Boletín de la Sociedad Geológica del Perú 61: 67-99.

Vicente, J.C. 1989. Early late Cretaceous overthrusting in the Western Cordillera of southern Peru. *In* Geology of the Andes and its relations to hydrocarbon and mineral resources (Ericksen, G.E.; Cañas, M.T.; Reinemund, J.A.; editors). Circum-Pacific Council for Energy and Mineral Resources Earth Science Series 11: 91-117. Houston, Texas.

Wasteneys, H.; Clark, A.; Farrar, E.; Langridge, R. 1995. Grenvillian granulite-facies metamorphism in the Arequipa Massif, Peru: a Laurentia-Gondwana link. Earth and Planetary Science Letters 132 (1-4): 63-73.

Weibel, M.; Frangipane-Gysel, M.; Hunziker, J.C. 1978. Ein Beitrag zur Vulkanologie Süd-Perus: Geologische Rundschau 67: 243-252.

Wilson, J.; García, W. 1962. Geología de los Cuadrángulos de Pachía y Palca (36v y 36x), Boletín Serie A: Comisión de la Carta Geológica Nacional: 81 p. Lima.

Wipf, M. 2006. Evolution of the Western Cordillera and Coastal Margin of Peru: Evidence from Low-temperature Thermochronology and Geomorphology. Ph.D. Thesis (Unpublished). Swiss Federal Institute of Technology Zürich: 163 p.

Manuscript received: March 04, 2017; revised/accepted: November 14, 2018; available online: February 04, 2019.

APPENDIX

TABLE A1. U-Pb ZIRCON ANALYTICAL DATA OBTAINED USING THE LA-ICP-MS METHOD.

Spot Name	ppm Total Pb	ppm ^{232}Th	ppm ^{238}U	^{232}Th/^{238}U	^{207}Pb/^{206}Pb	% ±1σ	^{207}Pb/^{235}U	% ±1σ	^{206}Pb/^{238}U	% ±1σ	rho	aparent ages						
												^{207}Pb/^{206}Pb	Ma ±1σ	^{207}Pb/^{235}U	Ma ±1σ	^{206}Pb/^{238}U	Ma ±1σ	% conc.
76-Orthogneiss																		
76-01	910,527	674,013	1.240,292	0,5434	0,107	0,0024	394,053	0,1343	0,2617	0,007	0,7352	1.742,6	40,74	1.622,0	27,6334	1.498,6	33,53	92
76-02	187,403	275,213	311,810	0,8826	0,075	0,0023	198,534	0,0644	0,1906	0,003	0,5191	1.076,9	59,73	1.110,5	21,9182	1.124,6	17,39	98
76-03	513,227	422,232	1.126,880	0,3747	0,092	0,0021	237,815	0,0595	0,1848	0,002	0,3676	1.465,1	42,60	1.236,1	17,8932	1.093,4	9,26	87
76-04	1.361,995	1.526,596	1.184,560	1,2887	0,099	0,0019	360,086	0,0877	0,2618	0,004	0,6162	1.596,0	35,18	1.549,7	19,3929	1.499,2	20,10	96
76-05	462,435	403,827	343,730	1,1748	0,112	0,0026	479,779	0,1119	0,3087	0,003	0,3963	1.831,5	42,28	1.784,5	19,6280	1.734,3	14,08	97
76-06	1.971,711	2.208,277	2.094,787	1,0542	0,105	0,0020	361,755	0,0757	0,2483	0,002	0,4618	1.707,1	35,19	1.553,4	16,6836	1.429,5	12,42	91
76-07	1.192,769	1.153,387	734,035	1,5713	0,107	0,0023	460,993	0,1051	0,3082	0,003	0,4537	1.766,7	38,58	1.751,1	19,0601	1.731,9	15,74	98
76-08	361,581	422,213	396,767	1,0641	0,092	0,0026	2,919	0,0878	0,2291	0,003	0,4090	1.465,7	55,09	1.386,8	22,7738	1.329,9	14,81	95
76-09	504,782	492,058	373,418	1,3177	0,103	0,0028	442,434	0,1203	0,3085	0,003	0,3733	1.684,9	82,41	1.716,9	22,5574	1.733,5	15,46	99
76-10	358,078	310,146	527,135	0,5884	0,098	0,0028	347,902	0,1247	0,2488	0,005	0,5594	1.594,4	56,48	1.522,5	28,2931	1.432,1	25,77	93
76-11	165,558	213,538	342,420	0,6236	0,081	0,0026	19,348	0,0636	0,1726	0,002	0,3164	1.213,9	62,96	1.093,2	22,0155	1.026,6	9,89	93
76-12	361,153	331,240	209,038	1,5846	0,114	0,0031	529,131	0,1484	0,3351	0,004	0,4092	1.865,7	48,92	1.867,5	23,9840	1.863,0	18,60	99
76-13	539,014	525,417	310,196	1,6938	0,108	0,0028	47,766	0,1217	0,3182	0,003	0,4092	1.773,8	46,30	1.780,8	21,4339	1.781,1	16,26	99
76-14	401,650	376,828	351,473	1,0721	0,105	0,0025	416,242	0,1047	0,2868	0,003	0,4219	1.705,9	44,29	1.666,7	20,6300	1.625,4	15,28	97
76-15	292,950	245,384	198,911	1,2336	0,114	0,0031	498,241	0,1427	0,3136	0,003	0,3747	1.933,3	49,69	1.816,3	24,2537	1.758,5	16,55	96
76-16	610,580	550,466	802,751	0,6857	0,092	0,0020	323,237	0,0924	0,2504	0,004	0,5437	1.457,7	41,51	1.465,0	22,1862	1.440,6	20,08	98
76-17	341,661	312,206	225,588	1,3840	0,102	0,0027	465,833	0,1178	0,3317	0,003	0,3947	1.654,6	48,61	1.759,8	21,1805	1.846,5	16,06	95
76-18	179,601	318,086	320,072	0,9938	0,094	0,0041	230,703	0,1024	0,1761	0,002	0,2261	1.505,6	81,79	1.214,5	31,4519	1.045,7	9,70	85
76-19	557,449	343,327	1.385,827	0,2477	0,089	0,0024	361,644	0,1488	0,2792	0,007	0,5756	1.416,7	50,01	1.553,2	32,7555	1.587,3	33,34	97
76-20	530,812	427,923	401,932	1,0647	0,108	0,0032	462,178	0,141	0,3058	0,003	0,3428	1.772,2	53,40	1.753,2	25,5036	1.720,0	15,82	98
77-Orthogneiss																		
77-01	16,262	30,309	85,208	0,356	0,06669	0,00460	1,48673	0,09045	0,16841	0,00297	0,29014	827,78	144,44	924,98	36,94	1.003,37	16,41	91
77-02	26,464	33,118	114,250	0,290	0,07414	0,00405	1,78547	0,09040	0,17968	0,00360	0,39536	1.055,56	110,04	1.040,18	32,96	1.065,24	19,66	97
77-03	29,495	50,861	153,756	0,331	0,06836	0,00293	1,54270	0,06555	0,16399	0,00234	0,33641	879,63	88,89	947,58	26,18	978,94	12,99	96
77-04	29,861	37,846	119,261	0,317	0,08920	0,00434	1,93533	0,09133	0,15949	0,00261	0,34730	1.409,26	88,43	1.093,38	31,60	953,91	14,54	86
77-05	20,635	26,056	108,075	0,241	0,08802	0,01261	2,16878	0,37854	0,17611	0,00337	0,10978	1.383,34	277,93	1.171,09	121,30	1.045,70	18,51	88
77-06	34,204	57,796	175,444	0,329	0,07357	0,00291	1,68776	0,06635	0,16644	0,00213	0,32530	1.029,32	81,02	1.003,92	25,07	992,46	11,77	98
77-07	67,821	119,772	299,626	0,400	0,07523	0,00243	1,79855	0,05645	0,17267	0,00187	0,34571	1.075,93	64,82	1.044,93	20,49	1.026,83	10,31	98
77-08	19,116	27,397	115,782	0,237	0,07724	0,00374	1,74724	0,08034	0,16493	0,00242	0,31846	1.127,79	96,30	1.026,14	29,70	984,12	13,38	95
77-09	41,319	60,113	199,333	0,302	0,07827	0,00282	1,95798	0,07102	0,18078	0,00288	0,43872	1.153,71	76,39	1.101,19	24,39	1.071,24	15,72	97
77-10	18,041	26,472	102,312	0,259	0,07950	0,00458	1,77767	0,09019	0,16630	0,00297	0,35177	1.184,88	114,04	1.037,33	32,98	991,67	16,41	95
77-11	32,776	51,446	122,751	0,419	0,08161	0,00455	1,79362	0,09463	0,16121	0,00247	0,29028	1.236,11	109,26	1.043,14	34,40	963,49	13,72	92
77-12	20,330	24,706	105,468	0,234	0,06772	0,00373	1,49397	0,08035	0,16138	0,00273	0,31404	861,11	114,81	927,93	32,72	964,46	15,14	96
77-13	143,164	244,859	578,835	0,423	0,07858	0,00208	2,05861	0,05589	0,18815	0,00206	0,40273	1.161,12	51,85	1.135,16	18,57	1.111,35	11,18	97
77-14	439,345	987,737	1.397,136	0,707	0,07528	0,00159	1,79147	0,03650	0,17082	0,00125	0,35973	1.075,93	42,28	1.042,36	13,30	1.016,64	6,92	97
77-15	196,700	275,275	1.013,765	0,272	0,07736	0,00163	1,94908	0,04089	0,18079	0,00145	0,38168	1.131,49	42,13	1.098,13	14,10	1.071,31	7,92	97
77-16	226,286	487,742	745,705	0,654	0,07701	0,00183	1,85743	0,04392	0,17335	0,00151	0,36824	1.121,30	47,68	1.066,07	15,62	1.030,53	8,31	96
77-17	161,901	305,235	609,069	0,501	0,07623	0,00183	1,91952	0,04674	0,18068	0,00159	0,36144	1.101,85	48,15	1.087,90	16,27	1.070,71	8,70	98
77-18	130,801	222,738	300,743	0,741	0,09085	0,00261	2,55786	0,07799	0,20162	0,00227	0,36876	1.443,52	55,40	1.288,68	22,27	1.184,01	12,18	91
77-19	271,708	643,432	806,072	0,798	0,07391	0,00186	1,74258	0,04410	0,16938	0,00169	0,39381	1.038,90	56,48	1.024,42	16,34	1.008,69	9,32	98
77-20	47,424	80,901	216,018	0,375	0,07454	0,00309	1,72452	0,07108	0,16773	0,00209	0,30185	1.057,41	84,42	1.017,71	26,50	999,59	11,53	98

Appendix table A1 continued.

Spot Name	ppm Total Pb	ppm ^{232}Th	ppm ^{238}U	^{232}Th/^{238}U	^{207}Pb/^{206}Pb	% ±1σ	^{207}Pb/^{235}U	% ±1σ	^{206}Pb/^{238}U	% ±1σ	rho	aparent ages ^{207}Pb/^{206}Pb	Ma ±1σ	^{207}Pb/^{235}U	Ma ±1σ	^{206}Pb/^{238}U	Ma ±1σ	% conc.
75-Quartz diorite																		
75-01	107,577	1.575,893	751,811	2,09613	0,051838	0,00289	0,22479	0,012	0,031398	0,0004	0,25809	279,69	160,17	205,89	9,929	199,29	2,70	96
75-02	178,816	2.733,879	1.039,186	2,63079	0,051601	0,00237	0,22370	0,0101	0,031291	0,0004	0,27083	333,39	100,91	204,98	8,345	198,62	2,38	96
75-03	614,932	819,034	607,193	1,34888	0,05246	0,00307	0,22844	0,0132	0,031331	0,0004	0,23171	305,62	135,17	208,91	10,935	198,87	2,63	95
75-04	346,234	5.653,242	1.915,336	2,95157	0,05035	0,00183	0,21741	0,0077	0,031038	0,0003	0,29158	209,33	87,95	199,75	6,437	197,04	2,01	98
75-05	141,475	1.995,540	977,685	2,04109	0,050382	0,00279	0,21998	0,0109	0,032097	0,0004	0,25703	213,04	132,39	201,89	9,058	203,66	2,55	99
75-06	901,069	1.338,714	715,126	1,87200	0,046143	0,00241	0,20249	0,0107	0,031702	0,0005	0,26811	400,05	272,19	187,23	9,058	201,19	2,82	92
75-07	107,547	1.605,213	777,782	2,06383	0,047332	0,00245	0,20519	0,0107	0,031153	0,0004	0,26301	64,91	118,51	189,51	9,024	197,76	2,68	95
75-08	169,928	2.440,495	1.132,164	2,15560	0,063251	0,00363	0,28266	0,0175	0,031532	0,0004	0,19584	716,68	122,21	252,76	13,860	200,13	2,39	76
75-09	103,164	1.441,664	863,503	1,66955	0,050425	0,00302	0,21540	0,0116	0,031376	0,0004	0,24994	213,04	134,24	198,08	9,65	199,15	2,63	99
75-10	101,861	1.398,328	857,089	1,63148	0,04578	0,00252	0,19982	0,0103	0,031953	0,0004	0,25092	error	-	184,97	8,72	202,76	2,59	90
75-11	114,818	1.677,404	881,666	1,90254	0,049009	0,00271	0,21257	0,0116	0,031342	0,0004	0,26171	150,09	129,61	195,71	9,68	198,94	2,79	98
75-12	399,111	584,466	618,568	0,94487	0,097764	0,00220	3,68205	0,0846	0,270937	0,0027	0,43270	1.583,34	47,06	1567,48	18,39	1.545,56	13,69	98
75-13	129,407	1.822,340	927,364	1,96508	0,05244	0,00266	0,23179	0,012	0,031955	0,0004	0,25355	305,62	116,65	211,67	9,87	202,77	2,62	95
75-14	131,225	1.954,248	995,423	1,96323	0,047387	0,00225	0,19697	0,0091	0,030083	0,0004	0,26331	77,87	111,10	182,56	7,69	191,07	2,28	95
75-15	218,127	3.157,272	1.247,168	2,53155	0,05069	0,00249	0,22048	0,011	0,031336	0,0004	0,24530	233,40	117,58	202,31	9,17	198,90	2,40	98
75-16	228,789	3.265,911	1.354,018	2,41201	0,050981	0,00216	0,21501	0,0087	0,030736	0,0003	0,28068	238,96	102,76	197,74	7,24	195,15	2,17	98
75-17	100,084	1.412,564	1.002,914	1,40846	0,051042	0,00268	0,21623	0,0106	0,031292	0,0004	0,27423	242,66	124,98	198,76	8,82	198,63	2,62	99
75-18	117,686	1.609,962	918,583	1,75266	0,047628	0,00290	0,20437	0,0118	0,03157	0,0004	0,24411	79,72	140,72	188,81	9,95	200,36	2,78	94
75-19	100,374	1.408,096	873,896	16,1129	0,051187	0,00276	0,21295	0,0116	0,030155	0,0004	0,23669	250,07	124,06	196,02	9,69	191,52	2,43	97
75-20	153,166	2.293,409	981,574	2,33646	0,048431	0,00288	0,20143	0,0113	0,030501	0,0004	0,24700	120,46	133,31	186,33	9,51	193,68	2,64	96
82-Diorite																		
82-01	315,593	3.502,748	2.019,393	1,734556	0,064646	0,0028	0,289958	0,0139	0,03176	0,0004	0,242711	762,66	60,18	258,53	10,95	201,55	2,31	75
82-02	100,232	1.353,733	725,055	1,867077	0,052727	0,0027	0,220743	0,0112	0,030338	0,0004	0,290473	316,73	116,65	202,53	9,33	192,66	2,80	95
82-03	164,242	1.923,429	1.280,511	1,50208	0,051337	0,0022	0,221276	0,0092	0,031273	0,0004	0,272475	257,47	98,13	202,97	7,64	198,51	2,21	97
82-04	52,279	427,185	286,607	1,490492	0,052955	0,005	0,207311	0,0174	0,030423	0,0006	0,233275	327,84	214,79	191,29	14,60	193,20	3,72	99
82-05	97,414	1.167,361	709,428	1,64547	0,056562	0,0031	0,24161	0,0127	0,031506	0,0004	0,24073	475,97	122,21	219,74	10,37	199,97	2,49	90
82-06	56,546	559,578	451,402	1,23965	0,06117	0,0041	0,257706	0,0168	0,031253	0,0005	0,262657	655,57	141,65	232,82	13,59	198,39	3,35	84
82-07	12.101,305	0	0	0	0,02367	0,0038	0,126207	0,0118	0,024592	0,0003	0,12813	error	error	120,68	10,65	156,62	1,86	74
82-08	136,910	1.308,169	804,029	1,627018	0,080467	0,0046	0,39178	0,0255	0,033376	0,0005	0,228944	1.209,26	112,19	335,67	18,61	211,64	3,11	54
82-09	162,167	1.932,777	1.251,114	1,544845	0,056303	0,0027	0,237922	0,0117	0,03086	0,0004	0,244994	464,86	107,40	216,72	9,56	195,93	2,32	89
82-10	63,008	662,568	644,777	1,027593	0,051431	0,0028	0,221154	0,0118	0,031562	0,0005	0,292068	261,18	128,69	202,87	9,78	200,32	3,07	98
82-11	206,608	2.631,565	1.507,509	1,745638	0,049024	0,0019	0,206804	0,0081	0,030726	0,0004	0,308439	150,09	92,58	190,87	6,85	195,09	2,33	97
82-12	411,863	3.581,831	2.263,384	1,582512	0,084642	0,0053	0,408924	0,0304	0,032623	0,0004	0,160916	1.307,10	118,05	348,10	21,94	206,95	2,44	49
82-13	769,774	10.407,978	5.152,240	2,020088	0,125234	0,0149	1,306083	0,2796	0,05148	0,0055	0,495648	2.032,41	211,57	848,40	123,13	323,60	33,49	10
82-14	702,496	9.943,927	4.778,629	2,080916	0,049608	0,0012	0,207626	0,0054	0,030188	0,0003	0,348421	176,01	59,25	191,56	4,55	191,72	1,72	99
82-15	276,830	3.940,983	1.865,787	2,112236	0,062943	0,0028	0,259917	0,0118	0,029744	0,0003	0,238867	705,57	94,44	234,60	9,54	188,95	2,03	78
82-16	293,990	3.865,224	1.947,415	1,984797	0,050754	0,0019	0,215894	0,0081	0,030933	0,0003	0,301091	227,85	91,65	198,49	6,76	196,38	2,19	98
82-17	100,663	1.014,216	601,693	1,685606	0,054395	0,0032	0,22667	0,0126	0,030827	0,0004	0,255305	387,09	136,10	207,45	10,40	195,72	2,73	94
82-18	33,643	193,218	185,538	1,041391	0,082254	0,0064	0,339812	0,025	0,030415	0,0006	0,266885	1.251,54	149,08	297,03	18,91	193,15	3,73	57
82-19	87,433	1.009,726	723,820	1,394996	0,050669	0,0035	0,205748	0,0126	0,030503	0,0004	0,228674	233,40	157,39	189,98	10,64	193,69	2,68	98
82-20	174,323	2.159,582	1.219,644	1,770666	0,048945	0,002	0,210236	0,0087	0,031089	0,0004	0,284622	146,38	98,13	193,75	7,31	197,36	2,30	98

Appendix table A1 continued.

Spot Name	ppm Total Pb	ppm ^{232}Th	ppm ^{238}U	^{232}Th/^{238}U	^{207}Pb/^{206}Pb	% ±1σ	^{207}Pb/^{235}U	% ±1σ	^{206}Pb/^{238}U	% ±1σ	rho	aparent ages ^{207}Pb/^{206}Pb	Ma ±1σ	^{207}Pb/^{235}U	Ma ±1σ	^{206}Pb/^{238}U	Ma ±1σ	% conc.
89-Tonalite																		
89-01	0,00585	0,05717	0,05910	0,96740	0,064026	0,0024	0,257321	0,0101	0,028581	0,0003	0,294342	742,60	79,62	232,51	8,14	181,66	2,07	75
89-02	0,01885	0,17075	0,21447	0,79614	0,058449	0,0024	0,23456	0,0099	0,028817	0,0003	0,266886	546,33	90,73	213,96	8,11	183,14	2,03	84
89-03	0,01789	0,17751	0,20730	0,85628	0,04837	0,0021	0,191169	0,0082	0,028267	0,0003	0,239217	116,76	101,84	177,63	7,01	179,69	1,83	98
89-04	0,03025	0,29166	0,33415	0,87285	0,047375	0,0018	0,18909	0,007	0,028743	0,0003	0,280982	77,87	75,92	175,85	5,97	182,68	1,87	96
89-05	0,00095	0,00809	0,00609	1,32723	0,082534	0,0029	0,371985	0,0148	0,031445	0,0004	0,303699	1.258,33	70,37	321,12	10,96	199,59	2,38	53
89-06	0,02693	0,24043	0,28168	0,85356	0,048764	0,0018	0,199264	0,0072	0,029485	0,0003	0,308854	200,08	82,40	184,50	6,09	187,32	2,06	98
89-07	0,00053	0,00482	0,00250	1,92618	0,133258	0,006	0,519735	0,023	0,0280019	0,0003	0,208619	2.142,59	78,55	424,97	15,34	178,14	1,62	18
89-08	0,02373	0,20774	0,27754	0,74853	0,054175	0,0025	0,217803	0,0098	0,029186	0,0004	0,282982	388,94	101,84	200,08	8,13	185,45	2,32	92
89-09	0,00383	0,03853	0,02986	1,29050	0,051428	0,002	0,208962	0,0079	0,029172	0,0003	0,292906	261,18	88,88	192,68	6,62	185,37	2,02	96
89-10	0,12568	1,37163	114,800	1,19480	0,047968	0,0021	0,186117	0,0079	0,028183	0,0003	0,288522	98,24	99,99	173,31	6,78	179,17	2,17	96
89-11	0,02806	0,31186	0,26031	1,19806	0,050867	0,0018	0,194399	0,0068	0,02763	0,0003	0,301256	235,25	83,32	180,38	5,80	175,70	1,84	97
89-12	0,39971	3,78655	457,717	0,82727	0,051202	0,0021	0,20334	0,0083	0,028715	0,0003	0,272632	250,07	94,43	187,95	7,01	182,50	2,01	97
89-13	0,04120	0,35205	0,41284	0,85273	0,05091	0,0022	0,215335	0,0089	0,030784	0,0004	0,301858	235,25	65,73	198,02	7,44	195,45	2,41	98
89-14	0,00749	0,07415	0,06526	1,13617	0,063834	0,0027	0,251397	0,0107	0,028143	0,0003	0,253264	744,45	94,59	227,71	8,67	178,92	1,90	76
89-15	0,00759	0,08125	0,07221	1,12517	0,052511	0,0022	0,204868	0,0082	0,028206	0,0003	0,28766	309,32	92,58	189,24	6,88	179,31	2,03	94
89-16	0,01437	0,13828	0,14343	0,96409	0,049715	0,0017	0,199844	0,0066	0,028928	0,0003	0,343247	188,97	77,77	184,99	5,59	183,83	2,06	99
89-17	0,06843	0,56398	0,85546	0,65927	0,056801	0,0027	0,226387	0,0106	0,028935	0,0004	0,296463	483,38	105,54	207,21	8,77	183,88	2,52	88
89-18	0,03494	0,33693	0,34228	0,98435	0,049218	0,002	0,196014	0,0081	0,028812	0,0003	0,271656	166,75	98,14	181,75	6,91	183,11	2,04	99
89-19	0,09244	0,93134	0,81294	1,14565	0,048036	0,0016	0,196826	0,0064	0,029779	0,0003	0,322501	101,94	77,77	182,44	5,42	189,17	1,95	96
89-20	0,01784	0,16733	0,20156	0,83019	0,050947	0,0019	0,201442	0,0073	0,028731	0,0003	0,303097	238,96	83,32	186,35	6,14	182,60	1,97	97
95A-Granodiorite																		
95A-01	93,717914	1.203,95	1.918,660	0,627497	0,048358	0,0019	0,192076	0,0074	0,028703	0,0003	0,285762	116,76	86,10	178,40	6,30	182,42	1,98	97
95A-02	133,48731	815,601	1.687,850	0,483219	0,051104	0,0019	0,204183	0,0076	0,028809	0,0003	0,291052	255,62	80,54	188,66	6,43	183,09	1,96	97
95A-03	57,071868	774,192	1.214,863	0,637267	0,051909	0,0024	0,199385	0,0091	0,027851	0,0003	0,25458	279,69	105,54	184,61	7,73	177,08	2,04	95
95A-04	104,95082	773,469	1.128,749	0,685245	0,07026	0,0033	0,299379	0,0155	0,029987	0,0004	0,265762	1.000,00	98,15	265,92	12,09	190,47	2,58	66
95A-05	138,82252	1.906,61	2.344,163	0,813344	0,050341	0,0016	0,20375	0,0065	0,02904	0,0003	0,292338	209,33	41,66	188,29	5,51	184,54	1,71	97
95A-06	62,132197	420,288	810,054	0,51884	0,051761	0,0027	0,203629	0,0101	0,028695	0,0004	0,270871	275,99	116,65	188,19	8,54	182,38	2,42	96
95A-07	103,88917	1.343,55	2.053,256	0,654351	0,051103	0,0019	0,207309	0,0077	0,029203	0,0003	0,278484	255,62	80,54	191,29	6,44	185,56	1,88	96
95A-08	74,712487	875,279	1.286,700	0,680251	0,052047	0,0023	0,204094	0,0089	0,028267	0,0003	0,254452	287,10	101,84	188,58	7,55	179,69	1,98	95
95A-09	62,657586	799,976	1.243,635	0,643257	0,050449	0,0022	0,196058	0,0084	0,027936	0,0003	0,266096	216,74	99,99	181,79	7,10	177,62	1,99	97
95A-10	43,445886	460,593	974,976	0,472415	0,050473	0,0024	0,194793	0,0088	0,028087	0,0004	0,288241	216,74	107,39	180,71	7,47	178,56	2,29	98
95A-11	71,368156	921,378	1.505,556	0,611985	0,051173	0,0022	0,203144	0,0088	0,028555	0,0003	0,274194	255,62	98,14	187,78	7,41	181,50	2,12	96
95A-12	45,480236	464,850	850,350	0,546658	0,051965	0,0028	0,214943	0,0115	0,029634	0,0004	0,248728	283,40	149,98	197,69	9,63	188,26	2,48	95
95A-13	35,830509	294,717	351,010	0,839627	0,07755	0,0056	0,299424	0,0191	0,028817	0,0005	0,272035	1.144,45	142,59	265,95	14,92	183,14	3,13	63
95A-14	80,435263	1.117,75	1.571,173	0,711411	0,051232	0,002	0,208643	0,0082	0,029219	0,0003	0,258376	250,07	86,10	192,41	6,92	185,66	1,87	96
95A-15	44,84881	343,036	594,268	0,577241	0,054051	0,0033	0,21016	0,0123	0,028422	0,0004	0,240295	372,28	137,02	193,69	10,28	180,67	2,50	93
95A-16	72,904234	939,232	1.451,802	0,646942	0,047614	0,0018	0,196189	0,0077	0,029454	0,0003	0,267488	79,72	88,88	181,90	6,50	187,13	1,93	97
95A-17	66,194238	911,009	1.274,082	0,715031	0,047348	0,0021	0,188328	0,0079	0,028648	0,0003	0,24956	77,87	90,73	175,20	6,72	182,08	1,87	96
95A-18	75,985769	795,175	1.265,643	0,628277	0,048656	0,0023	0,191944	0,0085	0,028601	0,0003	0,26082	131,57	111,10	178,29	7,28	181,79	2,08	98
95A-19	84,293857	684,325	1.221,106	0,560414	0,057191	0,0026	0,239551	0,0118	0,029636	0,0004	0,270153	498,19	101,84	218,05	9,64	188,27	2,47	85
95A-20	93,894539	1,224,033	1.795,427	0,68175	0,049306	0,0019	0,197942	0,0075	0,028849	0,0003	0,301679	161,20	86,10	183,38	6,39	183,34	2,08	99

Appendix table A1 continued.

Spot Name	ppm Total Pb	ppm ^{232}Th	ppm ^{238}U	$^{232}Th/^{238}U$	$^{207}Pb/^{206}Pb$	% ±1σ	$^{207}Pb/^{235}U$	% ±1σ	$^{206}Pb/^{238}U$	% ±1σ	rho	aparent ages						
												$^{207}Pb/^{206}Pb$	Ma ±1σ	$^{207}Pb/^{235}U$	Ma ±1σ	$^{206}Pb/^{238}U$	Ma ±1σ	% conc.
86-Tonalite																		
86-01	33,442794	547,138	715,623	0,764562	0,054247	0,0034	0,170415	0,0103	0,022729	0,0004	0,265425	388,94	140,73	159,78	8,98	144,88	2,31	90
86-02	49,974472	570,416	936,838	0,608874	0,069042	0,0038	0,21863	0,0113	0,023245	0,0004	0,299215	899,69	112,96	200,77	9,42	148,13	2,27	69
86-03	46,67413	755,383	1.000,319	0,755142	0,049247	0,0031	0,150367	0,0089	0,022674	0,0003	0,250824	166,75	-49,07	142,24	7,89	144,53	2,13	98
86-04	40,605717	693,464	872,080	0,795183	0,045649	0,0027	0,140266	0,0082	0,022322	0,0003	0,260507	error	-	133,28	7,35	142,31	2,16	93
86-05	47,780121	823,684	874,589	0,941795	0,049889	0,003	0,157871	0,0096	0,022998	0,0004	0,259202	190,82	140,72	148,84	8,46	146,58	2,30	98
86-06	40,787282	664,177	715,219	0,928634	0,051682	0,0036	0,159945	0,0106	0,023049	0,0004	0,249145	272,29	165,72	150,66	9,24	146,90	2,39	97
86-07	165,66397	3.251,463	2.481,275	1,3104	0,047063	0,0019	0,146381	0,0059	0,022567	0,0003	0,304072	53,80	92,58	138,71	5,20	143,86	1,73	96
86-08	55,771748	476,215	780,246	0,610339	0,142181	0,0105	0,527299	0,0404	0,025492	0,0005	0,25459	2.254,02	128,09	430,02	26,85	162,27	3,13	9
86-09	31,052135	522,184	682,894	0,764662	0,048516	0,0035	0,152075	0,0101	0,023393	0,0004	0,262856	124,16	162,94	143,74	8,90	149,06	2,57	96
86-10	34,586664	575,063	737,729	0,779505	0,057929	0,0039	0,174956	0,0109	0,022224	0,0004	0,263039	527,82	180,53	163,71	9,43	141,70	2,30	85
86-11	73,928451	1.267,142	1.494,589	0,84782	0,049808	0,0024	0,155915	0,0075	0,022708	0,0003	0,274823	187,12	108,32	147,12	6,63	144,75	1,90	98
86-12	63,667566	1.151,734	1.321,459	0,871562	0,046964	0,0025	0,142221	0,0071	0,022031	0,0003	0,272555	55,65	112,95	135,02	6,31	140,48	1,89	96
86-13	23,794698	430,034	513,328	0,837737	0,051963	0,0046	0,154373	0,0131	0,022844	0,0005	0,239486	283,40	197,20	145,77	11,49	145,60	2,92	99
86-14	73,907999	1.405,140	1.240,589	1,132639	0,056652	0,0029	0,171649	0,0086	0,022015	0,0003	0,267462	479,67	112,95	160,85	7,41	140,38	1,85	86
86-15	27,491569	448,812	606,539	0,739956	0,051705	0,0036	0,159995	0,0098	0,022962	0,0004	0,251701	272,29	163,87	150,70	8,58	146,35	2,23	97
86-16	64,232673	812,610	1.304,624	0,622869	0,067795	0,0035	0,2364	0,0131	0,024794	0,0004	0,28697	861,11	109,26	215,47	10,77	157,88	2,49	69
86-17	36,558705	632,976	766,150	0,826177	0,049245	0,0042	0,150891	0,0114	0,023372	0,0004	0,220829	166,75	183,31	142,70	10,10	148,93	2,47	95
86-18	95,133189	1.776,814	1.649,333	1,077293	0,043505	0,0021	0,138415	0,0066	0,023182	0,0003	0,252832	error	error	131,63	5,87	147,73	1,76	88
86-19	163,53927	3.203,723	2.035,733	1,573744	0,051338	0,0023	0,157426	0,007	0,022394	0,0003	0,255196	257,47	108,32	148,45	6,14	142,77	1,60	96
86-20	93,737332	1.793,900	1.607,434	1,116002	0,054523	0,0026	0,163866	0,0075	0,022081	0,0003	0,273855	394,50	107,40	154,08	6,57	140,79	1,76	90

TABLE A2. U-Pb ZIRCON ANALYTICAL DATA OBTAINED USING THE SHRIMP IIIE METHOD

Spot Name	Meas $^{204}Pb/^{206}Pb$	% err	Meas $^{207}Pb/^{206}Pb$	% err	Meas $^{208}Pb/^{206}Pb$	% err	ppm Th	ppm U	$^{232}Th/^{238}U$	Corr $^{206}Pb/^{238}U$	% err	ppm Rad ^{206}Pb	$^{207}corr$ $^{206}Pb/^{238}U$ Age	1σ err	$^{204}Corr$ $^{207}Pb/^{206}Pb$	% err	$^{204}Corr$ $^{207}Pb/^{235}U$	% err	$^{204}Corr$ $^{206}Pb/^{238}U$	% err	err corr.
Q-DIO-Quartz Diorite																					
Q-DIO-1.1	-0,000035	107,54	0,048	3,64	0,173	4,64	73,46	145,3	0,52	0,027	1,47	3,4	174,79	2,57	0,049	3,78	0,19	4,05	0,0275	1,47	0,363
Q-DIO-2.1	-0,000045	0,84	0,049	2,26	0,265	2,39	245,02	302,1	0,84	0,028	1,25	7,4	180,12	2,25	0,050	2,24	0,20	2,57	0,0283	1,25	0,489
Q-DIO-3.1	0,000145	24,81	0,051	2,08	0,344	1,97	342,94	320,6	1,11	0,029	1,24	8,0	184,55	2,27	0,048	2,51	0,19	2,80	0,0290	1,24	0,442
Q-DIO-4.1	0,000229	37,65	0,053	3,04	0,174	4,09	84,36	154,0	0,57	0,028	1,40	3,8	179,83	2,52	0,050	4,23	0,20	4,46	0,0283	1,41	0,316
Q-DIO-5.1	0,000018	919,16	0,049	2,61	0,274	3,17	226,59	246,1	0,95	0,029	1,30	6,0	181,65	2,37	0,049	5,61	0,19	5,77	0,0285	1,34	0,232
Q-DIO-6.1	0,000015	827,80	0,049	3,01	0,175	3,24	125,89	231,7	0,56	0,028	1,29	5,7	181,13	2,35	0,049	4,83	0,19	5,01	0,0285	1,32	0,263
Q-DIO-7.1	0,000120	38,91	0,051	2,45	0,183	3,14	136,57	244,3	0,58	0,028	1,29	5,9	178,40	2,30	0,050	2,94	0,19	3,21	0,0281	1,29	0,402
Q-DIO-8.1	0,000134	37,80	0,050	2,39	0,164	3,18	118,90	247,4	0,50	0,029	1,28	6,1	183,33	2,34	0,048	2,99	0,19	3,25	0,0288	1,28	0,394
Q-DIO-9.1	0,000016	101,57	0,051	2,41	0,207	3,58	148,72	238,6	0,64	0,028	1,28	5,8	178,96	2,29	0,051	2,47	0,20	2,78	0,0282	1,28	0,462
Q-DIO-10.1	0,000049	78,71	0,050	1,88	0,267	1,98	327,52	401,8	0,84	0,028	1,21	9,8	180,27	2,17	0,049	2,24	0,19	2,54	0,0284	1,21	0,475
Q-DIO-11.1	0,000000	0,00	0,048	3,51	0,184	4,66	85,61	139,3	0,63	0,027	1,46	3,2	170,62	2,50	0,048	3,51	0,18	3,80	0,0268	1,46	0,385
Q-DIO-12.1	0,000000	0,00	0,048	3,76	0,203	3,66	122,26	197,2	0,64	0,026	1,38	4,4	167,18	2,31	0,048	3,76	0,17	4,01	0,0262	1,38	0,344
Q-DIO-13.1	0,000152	73,38	0,050	2,87	0,192	3,55	100,40	167,7	0,62	0,028	1,42	4,0	178,31	2,53	0,048	4,60	0,19	4,82	0,0280	1,43	0,298
Q-DIO-14.1	0,000138	14,33	0,051	2,21	0,264	2,37	232,77	286,9	0,84	0,028	1,25	6,8	175,06	2,19	0,049	2,45	0,18	2,76	0,0275	1,25	0,455
Q-DIO-15.1	0,002241	37,18	0,083	11,96	0,297	8,56	156,72	241,6	0,67	0,029	1,28	6,1	179,67	3,38	0,050	34,17	0,19	34,30	0,0283	2,08	0,061
Q-DIO-12.2	0,000123	64,86	0,050	2,97	0,197	3,66	108,51	183,0	0,61	0,027	1,37	4,2	171,72	2,35	0,048	3,98	0,18	4,21	0,0269	1,38	0,326
Q-DIO-16.1	-0,000010	83,68	0,048	2,29	0,291	2,27	248,48	283,8	0,90	0,027	1,25	6,6	171,30	2,14	0,049	2,30	0,18	2,62	0,0269	1,25	0,480
Q-DIO-17.1	0,000035	50,00	0,075	1,59	0,151	1,74	174,02	350,2	0,51	0,174	1,14	52,3	1.031,11	11,40	0,075	1,64	1,79	1,99	0,1736	1,14	0,571
Q-DIO-18.1	0,000036	64,80	0,049	1,57	0,316	1,53	586,74	599,0	1,01	0,029	1,17	14,7	181,90	2,11	0,049	1,75	0,19	2,10	0,0286	1,17	0,556
Q-DIO-19.1	0,000090	147,01	0,051	2,31	0,196	2,87	160,82	258,6	0,64	0,028	1,27	6,2	176,98	2,24	0,050	4,62	0,19	4,80	0,0278	1,29	0,269
Q-DIO-20.1	0,000134	74,26	0,051	2,03	0,240	2,29	254,33	337,0	0,78	0,028	1,23	8,1	178,31	2,18	0,049	3,71	0,19	3,91	0,0280	1,24	0,317
ZAD-DIO-Quartz Monzodiorite																					
ZAD-DIO-1.1	0,000299	45,46	0,054	3,83	0,183	4,09	73,96018	134,46	0,57	0,028	1,42	3,2	175,97	2,52	0,0496	5,96	0,19	6,13	0,0277	1,44	0,235
ZAD-DIO-2.1	0,000006	1.046,12	0,050	2,18	0,191	2,70	181,8734	298,17	0,63	0,028	1,25	7,2	177,60	2,21	0,0499	2,88	0,19	3,14	0,0279	1,25	0,399
ZAD-DIO-1.2	0,000272	45,31	0,054	2,65	0,209	3,26	119,5844	194,89	0,63	0,029	1,34	4,9	183,87	2,46	0,0498	4,78	0,20	4,98	0,0289	1,36	0,273
ZAD-DIO-3.1	0,000167	37,81	0,052	2,65	0,237	3,01	133,9456	193,35	0,72	0,027	1,33	4,6	174,01	2,31	0,0493	3,44	0,19	3,69	0,0274	1,33	0,361
ZAD-DIO-4.1	0,000187	37,81	0,051	2,81	0,168	3,74	87,86189	181,34	0,50	0,028	1,35	4,3	174,55	2,35	0,0486	3,75	0,18	3,99	0,0274	1,35	0,339
ZAD-DIO-5.1	0,000004	2.830,50	0,050	2,24	0,191	2,77	202,6828	329,35	0,64	0,027	1,25	7,5	169,01	2,11	0,0499	3,94	0,18	4,14	0,0266	1,27	0,306
ZAD-DIO-6.1	-0,000045	78,21	0,049	2,44	0,250	2,69	191,4484	247,18	0,80	0,028	1,29	5,9	175,70	2,26	0,0498	2,63	0,19	2,93	0,0276	1,29	0,440
ZAD-DIO-7.1	0,000033	302,00	0,051	2,13	0,221	2,46	215,9371	322,14	0,69	0,028	1,28	7,7	176,80	2,26	0,0501	3,63	0,19	3,85	0,0278	1,29	0,336
ZAD-DIO-8.1	0,000138	151,25	0,050	3,38	0,166	4,39	63,03425	130,3	0,50	0,028	1,52	3,1	177,30	2,70	0,0484	7,32	0,19	7,49	0,0278	1,57	0,210
ZAD-DIO-9.1	0,000110	62,42	0,051	2,38	0,214	2,80	175,7438	262,13	0,69	0,029	1,28	6,5	182,95	2,33	0,0493	3,23	0,20	3,48	0,0288	1,28	0,369
ZAD-DIO-10.1	0,000000	0,00	0,049	3,13	0,232	3,55	112,6739	154,16	0,76	0,028	1,41	3,8	180,73	2,54	0,0494	3,13	0,19	3,43	0,0284	1,41	0,410
ZAD-DIO-11.1	-0,000007	1,24	0,050	3,35	0,213	4,14	95,30003	143,54	0,69	0,028	1,43	3,5	178,16	2,55	0,0497	3,34	0,19	3,63	0,0280	1,43	0,393
ZAD-DIO-12.1	-0,000026	70,54	0,050	2,06	0,283	2,11	307,5458	348,46	0,91	0,027	2,03	8,1	172,08	3,46	0,0501	2,12	0,19	2,93	0,0271	2,03	0,692
ZAD-DIO-12.2	0,000080	85,69	0,050	1,99	0,233	2,22	315,9783	429,81	0,76	0,028	1,21	10,2	176,36	2,13	0,0485	2,94	0,19	3,18	0,0277	1,22	0,383
ZAD-DIO-13.1	0,000221	34,77	0,052	2,12	0,200	2,62	182,3148	297,05	0,63	0,028	1,25	7,1	176,27	2,19	0,0489	3,37	0,19	3,60	0,0277	1,26	0,348
ZAD-DIO-14.1	-0,000029	0,77	0,050	2,53	0,234	2,82	157,0875	216,73	0,75	0,028	1,30	5,2	176,25	2,28	0,0507	2,51	0,19	2,82	0,0278	1,30	0,459
ZAD-DIO-15.1	-0,000133	1,28	0,050	2,36	0,304	2,34	227,9399	250,81	0,94	0,027	1,27	5,8	172,46	2,19	0,0519	2,32	0,19	2,65	0,0272	1,27	0,481
ZAD-DIO-16.1	-0,000011	107,53	0,049	2,44	0,168	3,21	126,7434	246,27	0,53	0,028	1,28	5,8	175,58	2,24	0,0493	2,46	0,19	2,77	0,0276	1,28	0,461
ZAD-DIO-17.1	0,000074	72,78	0,052	1,99	0,240	2,28	280,434	361,69	0,80	0,028	1,48	8,6	176,09	2,59	0,0508	2,59	0,19	2,98	0,0277	1,48	0,497
ZAD-DIO-11.2	-0,000065	68,85	0,049	2,69	0,208	3,16	151,115	228,5	0,68	0,028	1,51	5,4	176,54	2,66	0,0498	2,96	0,19	3,33	0,0278	1,52	0,456
ZAD-DIO-18.1	-0,000038	61,24	0,049	2,08	0,200	2,68	197,642	313,81	0,65	0,027	1,27	7,4	174,17	2,20	0,0495	2,18	0,19	2,52	0,0274	1,27	0,503

Appendix table A1 continued.

Spot Name	Meas $^{204}Pb/^{206}Pb$	% err	Meas $^{207}Pb/^{206}Pb$	% err	Meas $^{208}Pb/^{206}Pb$	% err	ppm Th	ppm U	$^{232}Th/^{238}U$	Corr $^{206}Pb/^{238}U$	% err	ppm Rad ^{206}Pb	^{207}corr $^{206}Pb/^{238}U$ Age	1σ err	^{204}Corr $^{207}Pb/^{206}Pb$	% err	^{204}Corr $^{207}Pb/^{235}U$	% err	^{204}Corr $^{206}Pb/^{238}U$	% err	err corr.
M-DIO-Microdiorite																					
M-DIO-1.1	6,283E-05	112,3	0,0569	1,603	0,0599	3,74	40,35	194,53	0,2143	0,0775	1,24	12,96	480,88	5,78	0,06	2,47	0,598	2,77	0,0774	1,25	0,4506
M-DIO-2.1	8,163E-05	56,8	0,0546	1,610	0,0800	2,37	134,67	527,22	0,2639	0,0524	1,18	23,71	328,48	3,78	0,05	2,10	0,385	2,41	0,0523	1,18	0,4887
M-DIO-3.1	1,073E-04	109,2	0,0540	2,114	0,2454	2,42	140,79	182,38	0,7976	0,0510	1,28	7,99	319,90	4,06	0,05	3,96	0,368	4,17	0,0509	1,30	0,3125
M-DIO-4.1	-2,129E-05	0,3	0,1075	0,620	0,1096	1,41	69,47	184,62	0,3888	0,3095	1,32	49,09	1.738,98	20,10	0,11	0,62	4,604	1,46	0,3096	1,32	0,9053
M-DIO-5.1	2,502E-05	28,4	0,1076	0,500	0,3433	0,57	475,10	406,94	1,2063	0,3104	1,13	108,51	1.741,86	17,30	0,11	0,51	4,590	1,24	0,3102	1,13	0,9113
M-DIO-6.1	8,937E-06	196,3	0,0568	1,231	0,0293	4,05	29,86	329,49	0,0937	0,0771	1,20	21,82	478,70	5,53	0,06	1,31	0,602	1,78	0,0771	1,20	0,6738
M-DIO-7.1	2,408E-05	44,5	0,1084	0,654	0,3963	0,82	208,67	153,68	1,4030	0,3225	1,21	42,58	1.801,45	19,07	0,11	0,67	4,804	1,39	0,3224	1,21	0,8750
M-DIO-1.2	4,290E-05	152,3	0,0572	1,994	0,1653	2,52	82,39	158,43	0,5373	0,0771	1,27	10,50	478,59	5,89	0,06	2,63	0,601	2,93	0,0771	1,28	0,4365
M-DIO-8.1	6,445E-05	45,0	0,0760	0,911	0,0333	2,93	43,84	409,58	0,1106	0,1797	1,14	63,24	1.064,21	11,20	0,08	1,09	1,858	1,58	0,1795	1,14	0,7236
M-DIO-8.2	1,163E-05	38,9	0,0860	0,603	0,0520	8,77	57,00	381,25	0,1545	0,2033	1,27	66,60	1.193,02	13,84	0,09	0,61	2,406	1,41	0,2033	1,27	0,9015
M-DIO-9.1	8,047E-05	33,3	0,0806	0,662	0,3168	0,91	339,93	328,83	1,0681	0,2046	1,15	57,79	1.198,13	12,58	0,08	0,85	2,239	1,43	0,2043	1,15	0,8043
M-DIO-9.2	3,788E-05	46,9	0,0795	0,810	0,1304	1,68	96,90	215,12	0,4654	0,2017	1,18	37,28	1.183,91	12,77	0,08	0,88	2,196	1,47	0,2016	1,18	0,8016
M-DIO-10.1	1,360E-03	30,2	0,0690	5,199	0,3135	2,82	195,27	257,76	0,7828	0,0290	1,34	6,42	179,66	2,76	0,05	15,8	0,191	15,89	0,0283	1,56	0,0983
M-DIO-11.1	9,870E-05	61,7	0,0560	0,971	0,0674	2,11	124,32	619,86	0,2072	0,0635	1,15	33,82	396,21	4,43	0,05	1,95	0,477	2,26	0,0634	1,15	0,5089
M-DIO-12.1	6,680E-05	40,8	0,1065	1,170	0,4248	1,36	219,51	150,34	1,5087	0,3042	1,20	39,29	1.710,23	18,11	0,11	1,24	4,425	1,73	0,3038	1,21	0,6971
M-DIO-13.1	8,609E-05	38,7	0,0809	0,590	0,2760	0,77	349,20	398,96	0,9044	0,1949	1,13	66,81	1.146,28	11,92	0,08	0,87	2,139	1,43	0,1946	1,13	0,7935
M-DIO-14.1	1,661E-04	57,0	0,1073	1,090	0,3996	1,65	102,26	75,91	1,3920	0,2778	1,85	18,12	1.575,92	25,97	0,11	1,69	4,010	2,52	0,2769	1,86	0,7388
M-DIO-3.2	1,256E-04	34,2	0,0522	1,787	0,2967	1,84	244,99	260,37	0,9722	0,0509	1,22	11,38	319,08	3,82	0,05	2,30	0,353	2,60	0,0507	1,23	0,4706